PNL-10761
UC-721

Effect of Colloidal Aggregation on the Sedimentation and Rheological Properties of Tank Waste

D. R. Rector
B. C. Bunker

September 1995

Prepared for the U.S. Department of Energy
under Contract DE-AC06-76RLO 1830

Pacific Northwest Laboratory
Operated for the U.S. Department of Energy
by Battelle Memorial Institute

PNL-10761

PACIFIC NORTHWEST LABORATORY
operated by
BATTELLE MEMORIAL INSTITUTE
for the
UNITED STATES DEPARTMENT OF ENERGY
under Contract DE-AC06-76RLO 1830

Printed in the United States of America

Available to DOE and DOE contractors from the Office of Scientific and Technical Information, P.O. Box 62, Oak Ridge, TN 37831; prices available from (615) 576-8401.

Available to the public from the National Technical Information Service, U.S. Department of Commerce, 5285 Port Royal Rd., Springfield, VA 22161

PNL-10761
UC-721

Effect of Colloidal Aggregation on the Sedimentation and Rheological Properties of Tank Waste

D. R. Rector
B. C. Bunker

September 1995

Prepared for
the U.S. Department of Energy
under Contract DE-AC06-76RLO 1830

Pacific Northwest Laboratory
Richland Washington 99352

Summary

Many steps in the processing of hazardous tank wastes involve the handling of complex suspensions consisting of slurries of insoluble colloidal particles. The current baseline process for tank waste remediation involves steps including sluicing to create sludge suspensions, transporting the suspensions via pumping to central processing facilities, washing and leaching, and separating particles from supernatant liquids to form high and low level waste streams. In all of the above steps, process optimization requires controlling how the colloidal particles in sludge suspensions interact with each other to influence key slurry properties.

Tank farm experience and work performed under the Tank Waste Treatment Science task of the Tank Waste Remediation System (TWRS) Pretreatment Technology Development Project indicate that colloidal interactions can have an enormous impact on tank waste processing. For example, solids loadings desired for retrieval and transport need to be as high as possible to minimize waste volumes. However, work done on sludges and single sludge components suggests that some systems form shear-thinning gels at high solids loadings with viscosities greater than 10,000 centipoise. For some sludge components, solids loadings need to be kept below 1 wt% to keep slurry viscosities below 100 centipoise for pumping. High solids loadings are desired in settle-decant operations to minimize contaminants entrapped in interstitial liquids and to maximize the use of limited available processing volumes. In addition, rapid sedimentation velocities (greater than 3 cm/hr) are desired to allow solid liquid separations to be achieved in a reasonable time frame. Unfortunately, laboratory experiments on sedimentation suggest that low density sediments can form with negligible sedimentation velocities at solids loadings as low as 4 wt%. In some cases, sedimentation results observed in small lab-scale tests are not consistent with observations made in actual tanks. More seriously, many of the key sludge properties, such as viscosity, sedimentation rate, and sediment density, can vary by as much as an order of magnitude from tank to tank or even from process to process on the same sludge sample.

Given the wide range of compositions, particle types, and solution chemistries represented by Hanford tank wastes, one might conclude that explaining the wide range of behaviors observed for sludge suspensions represents an impossible task. Fortunately, there are some general principles that apply to all sludge suspensions. All of the property variations observed to date are the result of the formation of and interactions between colloidal aggregates.

This report provides the theoretical and experimental background required to understand how such agglomeration phenomena control the sedimentation and rheological behavior of colloidal tank wastes. First, the report describes the conditions under which the colloidal particles present in tank sludge are expected to aggregate. Computational models have been developed to predict solution conditions leading to agglomeration, and to predict the rate and size of aggregate growth. The models show that tank sludge should be heavily agglomerated under most baseline processing conditions. Second, the report describes models used to predict sedimentation rates and equilibrium sediment density profiles based on knowledge of agglomerate structures. The sedimentation models provide a self-consistent picture that explains the apparent discrepancies between bench-top experiments and tank-farm

experience. Finally, both discrete and empirical models are presented that can be used to rationalize and predict the rheological properties of colloidal sludge suspensions. In all cases, model predictions are compared and contrasted with experimental results. The net results indicate that most of the observed behaviors of real sludges can be predicted, understood, and perhaps ultimately controlled by understanding a few key central concepts regarding agglomeration phenomena.

Acknowledgments

The authors wish to thank J.P. LaFemina for his guidance and support. They also acknowledge the valuable contributions from the members of the Colloidal Science Task, including P. J. Briunsma, G. L. Graff, C. R. Hymas, X. S. Li, J. R. Phillips, P. A. Smith, and L. Song.

Contents

Figures

Tables

1.0 Introduction

The nuclear wastes currently stored in tanks at the Hanford Site contain complex mixtures of insoluble sludge particles, salts, and supernatant liquids. Treatment and ultimate disposal of these tank wastes will require that the complex solid-liquid mixtures be dispersed in aqueous solutions for retrieval and transport. The mixtures will then require pretreatment steps that will ultimately require the isolation of insoluble particles from supernatant liquids via solid-liquid separation steps such as settle-decant operations, centrifugation, or filtration. There is a perception both among the general public and the U.S. Department of Energy (DOE) that sludge treatment in general, and both transport and solid-liquid separations in particular, are relatively trivial operations that can easily be transferred to private industry to initiate tank cleanup. Unfortunately, experiences gained over the past few years at Hanford suggest otherwise.

The difficulties of tank waste processing can be illustrated by considering a process that appears to be completely mundane: separation of solid particles from supernatant liquids via sedimentation. In this process, a slurry of particles in an aqueous solution generated after transporting, washing, or leaching the sludge is left alone in a storage tank. Over time, the solid particles sink to the bottom by gravity. Ideally, this process yields a dense layer of particles on the bottom of the collection tank with a clear layer of supernatant liquids at the top of the tank. Solid-liquid separation is then readily achieved by merely pumping off the supernatant liquids and leaving the solids behind. Unfortunately, practical experience on both real sludge and on simulants reveals that the "ideal" sedimentation process is not often observed and that many key issues in sedimentation need to be understood and controlled.

The total volume occupied by the sediment layer needs to be minimized to reduce the capacity requirement of processing facilities (involving million-gallon tanks in the best-case scenario). In addition, the efficiency of the solid-liquid separation process depends on how effectively the particles in the sediment pack. The total volume of liquid in the tank is partitioned between supernatant liquids that can be pumped away and interstitial liquids that are trapped in the sediment layer. Even if the washing or leaching steps completely dissolve the desired constituents during processing, the fraction of the solubilized components actually removed in solid-liquid separations is limited to the fraction of the total liquids that are supernatant. Ideally, the goal is to have the sediment achieve maximum packing densities (as high as 60 vol% solids) to minimize the volume of interstitial liquids. In practice, sediment densities seem to span a range from 20 vol% down to as low as 5 vol%. The final sediment density also appears to be sensitive to both the nature of the sludge and to a wide range of processing parameters. For example, washing and leaching steps can transform a relatively dense sludge into a sediment that occupies 4 to 5 times its original volume. If such expansion is not controlled, or at least anticipated, the results in terms of waste processing could be quite serious.

Another process that appears to be completely mundane is the retrieval and transport of tank sludge before pretreatment. The main processing goal is to be able to produce low viscosity solutions (< 60 cP) that have the highest possible loadings of suspended particles. Low viscosity suspensions are required to insure that fluids can be pumped and that transfer lines are not plugged. High solids loadings are required to minimize the volume of waste to be treated. Experience has shown that some suspensions with solids loadings of over 10 vol% can meet these criteria. However, other suspensions

with less than 3 vol% solids loading can form a gel that can exhibit viscosities in excess of 25,000 cP. The rheological properties of these suspensions appear to depend not only on the particles in the suspension but also on the solution chemistry as well.

Given the complexity of Hanford wastes and the wide range of potentially variable processing parameters, one might assume that we will never be able to predict, understand, or control sedimentation or rheological behaviors. However, it appears that some relatively simple concepts can be used to rationalize the behavior of tank wastes. One concept that is central to understanding the behavior of sludge is the recognition that the observed behavior is typical of the behavior of agglomerates that are made up of fine particles. Transmission electron microscopy (TEM) shows that much of the material in sludge consists of extremely fine (5-10 nm) primary particles. If the particles are dispersed, they are too small to settle. If the particles stick to each other, they form larger agglomerates that can lead to most of the sedimentation and rheological behaviors described above.

The purpose of this report is to describe the effect of colloidal agglomeration on the sedimentation and rheological properties of Hanford tank waste, from both an experimental and a modeling perspective. The work presented here was performed by Pacific Northwest Laboratory (PNL) for Westinghouse Hanford Company (WHC) under the Tank Waste Treatment Science task through the TWRS Pretreatment Technology Development Project. Much of the experimental and theoretical modeling results have already been presented in the Tank Science quarterly reports (LaFemina et al. 1995a, 1995b, 1995c) and the reader is referred to them for further information.

Colloidal agglomeration is described in Section 2.0, along with models to predict suspension stability and aggregation kinetics. The effect of colloidal agglomeration on sedimentation behavior, along with computation models that have been developed to predict this behavior, is discussed in Section 3.0. The effect of colloidal agglomeration on rheological behavior is discussed in Section 4.0. Finally, in Section 5.0, we discuss the implications of this work on Hanford tank waste processing.

2.0 Colloidal Aggregation

Particles are considered colloidal when they are sufficiently small (and the corresponding surface-to-volume ratio is sufficiently large) that surface forces become important in determining the properties of the suspension. For many systems, this occurs at particle diameters of less than approximately 1 μm. In this section, we discuss the types of particles to be expected in Hanford tank waste, the driving forces behind particle aggregation, and computation models that are used to predict suspension stability and aggregation kinetics.

2.1 Characterization of Hanford Tank Waste Particulates

Elemental analysis of tank sludges indicates that the major insoluble components expected to be present are oxides and hydroxides of Al, Fe, Zr, and Cr, aluminosilicate minerals, and insoluble salts such as calcium phosphates (See Table 1; taken from Orme 1995). Particle images obtained via TEM provide information about the size and shape of particles that have different compositions. A TEM micrograph shown in Figure 1 for NCRW waste from Tank 105-AW shows a variety of nanoparticles of many phases and compositions. The TEM images reveal that while a broad range of particle sizes is present, over 50 vol% of the insoluble material in tank sludge is present as crystallites that are smaller than 1 μm in diameter.

The most important chemical constituent in sludge from a processing standpoint is probably aluminum because it is present in large quantities. Although it is relatively soluble in high pH solutions representative of tank wastes, it is present in sufficiently high concentrations that it can be present predominantly in the form of insoluble colloidal particles, as soluble species, or as mixtures of both depending on total aluminum present and on solution parameters such as pH and temperature. Even for a single tank solution, changes in processing conditions can lead to either dissolution or reprecipitation of the aluminum-containing particles present. TEM analyses suggest that aluminum is present in

Table 1. Major Components in Hanford Tank Waste

Element	Soluble Mass (MT)	Insoluble Mass (MT)	Total Mass (MT)
NA^{+}	67,800	777	68,500
Al^{+3}	1,980	2,550	4,530
PO_4^{-3}	3,110	1,850	4,970
Zr^{+4}	4.31	683	687
Fe^{+3}	31.8	761	793
Si^{+4}	15.9	232	248
Cr^{+3}	193	160	353

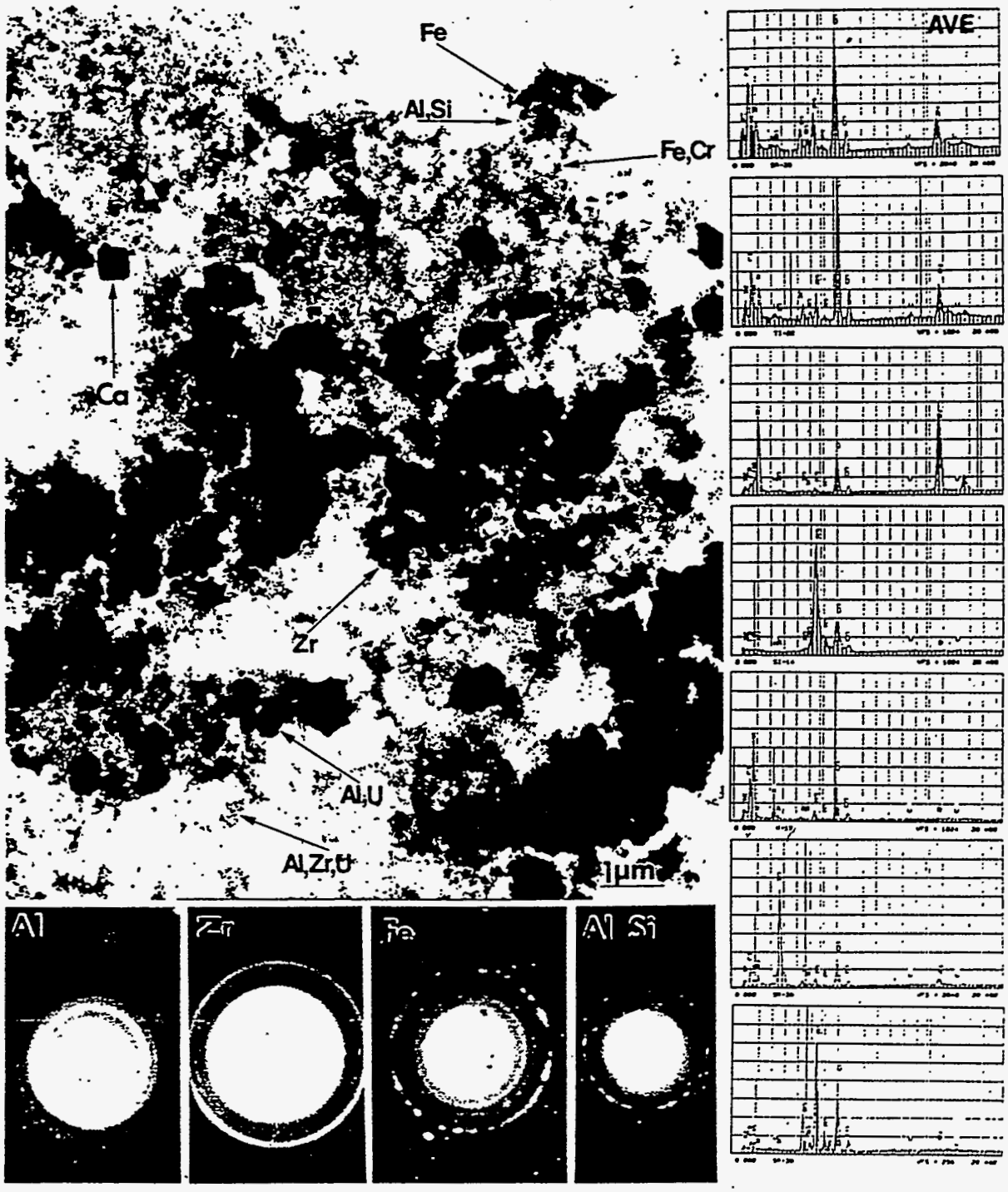

Figure 1. Transmission Electron Micrograph of NCRW Sludge from Tank 105-AW

three major forms: as extremely fine particles (< 10-nm crystallites) of boehmite [AlOOH], as 1- to 40-μm particles of gibbsite [$Al(OH)_3$], and as aluminosilicate clay-like minerals that are submicron in size.

Another important chemical constituent in tank sludge is iron, especially in the form of iron hydroxide [$Fe(OH)_3$]. $Fe(OH)_3$ and boehmite are similar because both materials exhibit similar surface charge characteristics (with isoelectric points between pH 9-10) and both contain submicron primary articles. Major differences between the particles are: 1) the primary particles in $Fe(OH)_3$ are equiaxed rather than plate-like, 2) the $Fe(OH)_3$ forms 1.6-μm agglomerates that are difficult to disperse regardless of solution conditions, and 3) the $Fe(OH)_3$ is less soluble than AlOOH at all pH values.

Although techniques such as TEM clearly show that most of the primary particles (by both number and volume percent) in real tank sludges are smaller than 0.1 μm in diameter, indirect measures of particle size using techniques such as sedimentation and light scattering indicate that most of the particles are larger than 1 μm. The apparent discrepancy between the two sets of measurements is due to the fact that under many slurry conditions, the primary particles are heavily agglomerated. However, *it is critical to understand that an agglomerate with an effective diameter of 1 μm does not behave anything like a primary particle having the same diameter*. Predictions based either on normal particle size distributions or on TEM results alone can be equally misleading.

In general, the material in sludge can be viewed on a wide range of length scales, each of which provides useful information regarding ultimate properties (Figure 2). At the smallest length (probed by TEM), the size of the primary particles can be determined. TEM images suggest that many of the primary particles in sludge are as small as 5-10 nm. Under many processing conditions, the primary particles agglomerate to form fractal clusters. The sizes of these clusters typically range from around 0.1 μm to a few microns in diameter. On a larger length scale, the fractal clusters can associate to form flocs that can range anywhere from 10 μm up to particles larger than 1 mm. The size of the large flocs is usually determined by the level of shear and Brownian motion in the solution, which tends to break up the larger flocs. Shear can also partially disrupt the smaller fractal clusters.

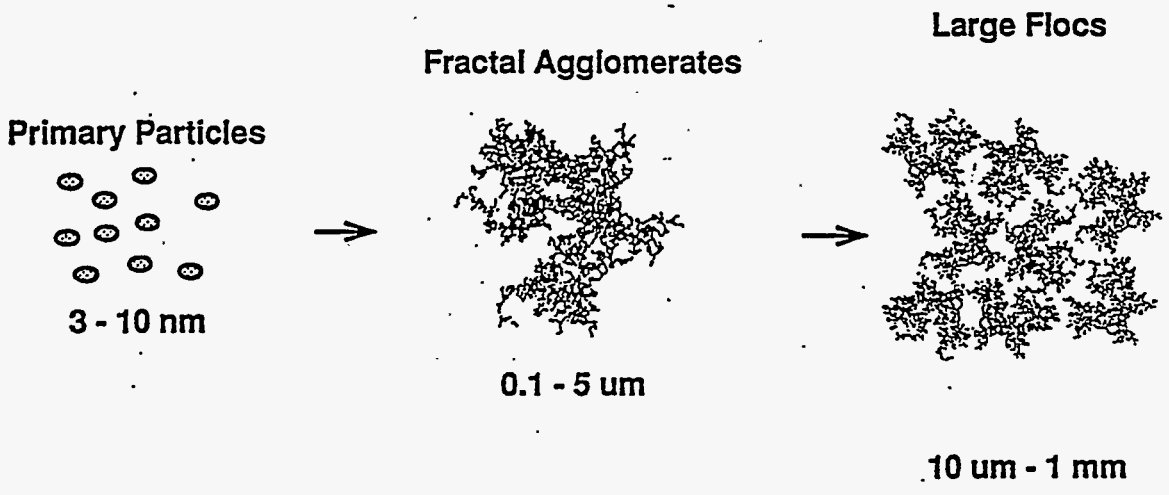

Figure 2. Particle Types in Tank Sludge

2.2 Particle-Particle Interactions

In simple electrolyte solutions, primary particles can either be dispersed or agglomerated, depending on the particle-particle interactions, or the potential energy between two particles. For example, under certain chemical conditions, colloidal particles repel each other and, if they are small, they may remain dispersed indefinitely. If the chemical conditions change, i.e., the pH changes or the salt concentration increases, the particles attract each other and form aggregates or gels. These forces can be explained using the DLVO (Derjaguin, Landau, Verwey and Overbeek) theory (Hunter 1986). This theory simply states that the total interaction between two particles consists of a van der Waals attraction term and an electrostatic term. The relative magnitude of these two terms determines the stability of the colloidal dispersion.

The van der Waals attraction term arises from the fact that each atom in a particle exerts an attractive force on each atom in an adjacent particle. The attractive potential energy, V_A , is given by the product of a term that depends only on the materials of the two particles and surrounding fluid, known as the Hamaker constant (Hunter 1986), and a term that describes the geometry of the two particles. For example, the attractive potential energy for two spheres of equal radius, R, at small separations, s, is given by

$$V_A = \frac{AR}{12s} \tag{1}$$

where A is the Hamaker constant. Such attractions will cause particles to stick to each other when they come within a few nanometers of each other. While van der Waals attractions can be strong at short distances (< 10 nm), the attraction becomes negligible for particles that are far apart.

The electrostatic term arises from charges created at particle surfaces due to adsorption or desorption of species such as protons and hydroxide ions. For oxides, the charges can be positive or negative depending on the solution pH and the acid-base properties of the surface. To satisfy electroneutrality, each charged surface is charge compensated by a cloud of ions extending into the solution (the electrical double layer). The counterion clouds interact, resulting in what is referred to as the double layer interaction (V_R). In dilute electrolyte solutions, the counterion clouds can extend far from the particle surface, making the double layer interaction a long-range interaction.

The length scale of the double layer interaction is characterized by the inverse Debye length, k, given by

$$\kappa^2 = \frac{2e^2 c\, z^2 N_A}{\epsilon\, k_B T} \tag{2}$$

where e is the electronic charge, c is the electrolyte concentration, z is the electrolyte charge, N_A is Avogadro's number and ϵ is the dielectric permittivity. The electrostatic potential energy for two

$$V_R = 2\pi\epsilon R\psi_0^2 \ln[1+\exp(-\kappa s)] \tag{3}$$

for kR> >1. Note that the electrostatic term depends both on the surface potential, ψ_0, which in turn depends on the pH of the solution and the salt concentration, c.

The DLVO pair potential is the sum of the van der Waals attraction term and the electrostatic term

$$V_T = V_A + V_R \tag{4}$$

Figure 3 shows an example of V_T as a function of separation. For the case of a large surface potential and low salt concentration, the repulsive electrostatic term dominates and there is a large potential barrier to aggregation. As the electrolyte concentration is increased, the Debye length increases (k decreases) and the attractive term becomes increasingly dominant (see Figure 4). Note that for a range of salt concentrations, a shallow secondary minimum forms which results in the loose flocculation of particles. When enough salt is added, the potential is purely attractive, resulting in the rapid aggregation of colloidal particles.

To predict the extent of agglomeration, the conditions leading to the formation of fixed charges on the particle surface need to be established. For this work, surface charge (or zeta potential) has been measured as a function of pH using electrophoretic mobility measurements (both alternating and direct current). The zeta potential measurements (Figure 5) show that boehmite has an isoelectric point (pH at which the surface is neutral) of between pH 8.5 and 9.0. Below pH 7, the surface has a substantial positive charge, while above pH 10, the surface has a substantial negative charge.

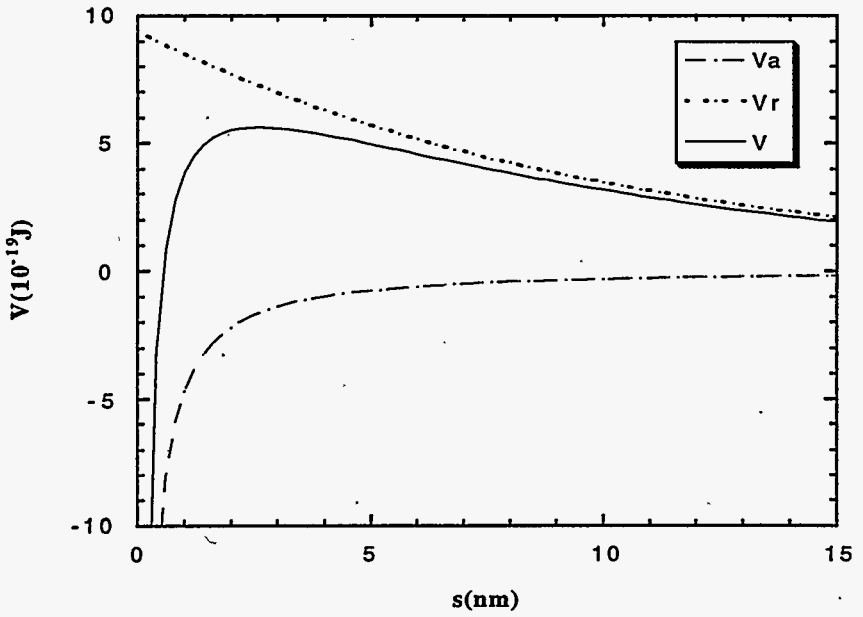

Figure 3. DLVO Potential as a Function of Separation

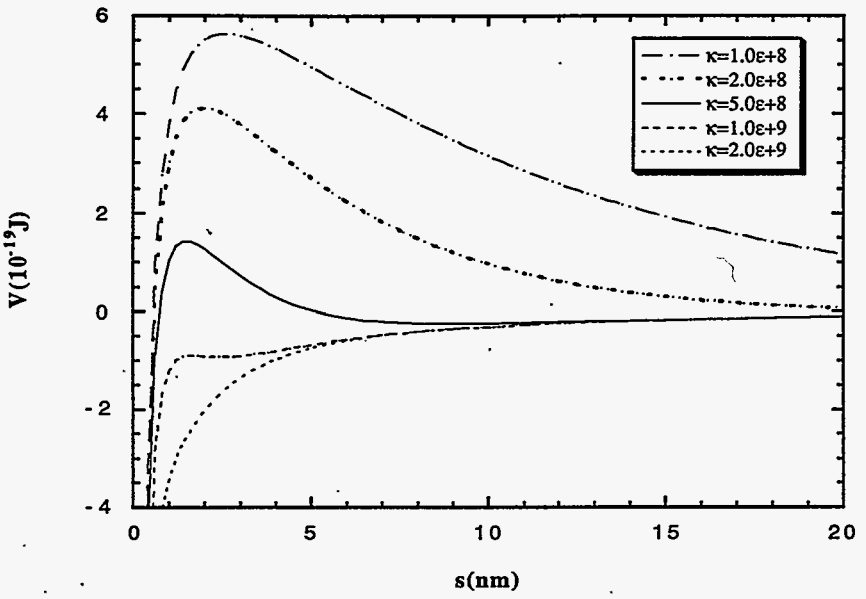

Figure 4. Effect of Inverse Debye Length on DLVO Potential

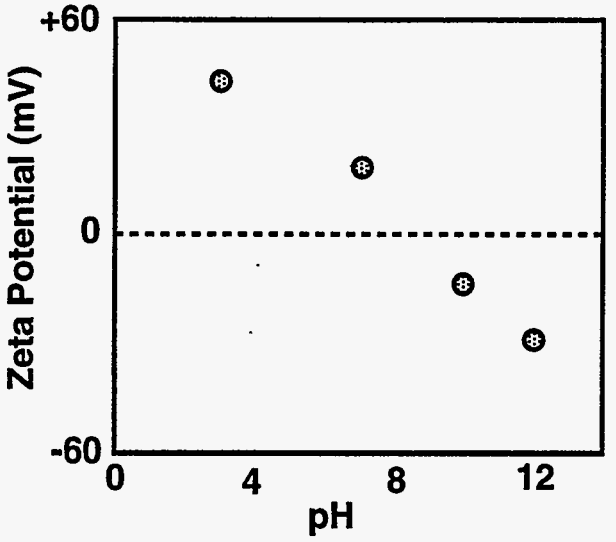

Figure 5. Surface Charge of AlOOH

The effect of surface charge on agglomeration has been determined for boehmite suspensions by measuring the agglomerate size distribution using light-scattering techniques (Figure 6). For boehmite, the particles are completely dispersed near pH 3 (all particles are positively charged), leading to an agglomerate size that is almost identical to the primary particle size of 50 nm. At pH 7 (near the isoelectric point), the particles have little surface charge, and the primary particles stick to each other to form large agglomerates (50 μm). At pH 13, one might expect to see primary particles, because all particles are negatively charged. However, the particles are somewhat agglomerated (around 1 μm in size) due to the high salt content (0.1 M NaOH) of the pH 13 solution. In terms of tank waste processing, the agglomeration study shows that particle interactions that control properties to be discussed in the following sections can be turned on and off by changes in solution chemistry. In addition, the results show that in the absence of TEM data, particle size distributions are of limited use, because such distributions normally probe agglomerate sizes and not primary particle sizes. As will be shown, agglomerates and primary particles that have similar sizes do not exhibit similar properties.

2.3 Colloidal Suspension Stability Maps

A colloidal dispersion is said to be stable when significant particle aggregation does not occur, that is, when the potential barrier described in the previous section is sufficiently high to prevent particles travelling at thermal Brownian velocities from contacting each other. Whether a dispersion is stable depends on both the surface electrostatic potential (which depends on the pH of the solution) and the ion concentration of the solution. By using the expressions for the DLVO particle interaction potential presented in the previous section, we are able to determine under which conditions the dispersion is stable or unstable.

The net interaction potential between particles can be used to predict the pH and salt concentration regimes expected to promote agglomeration. For example, one can assume that agglomeration can occur when the repulsive barrier to agglomeration is less than or equal to the thermal energy in the system (k_BT). (Even at 10 k_BT, a value commonly used by ceramic engineers, a significant number of particles have sufficient thermal energy to cross the repulsive barrier and agglomerate.)

Figure 7 shows the pH and salt concentration (for a 1:1 electrolyte such as $NaNO_3$) for which the barrier height is equal to k_BT for pairs of boehmite particles. The stability curve shows that near the isoelectric point at pH 8.5 (where the boehmite particles are neutral), agglomeration should occur regardless of the salt concentration. As the salt concentration increases, the instability regime widens. For $NaNO_3$ concentrations exceeding 0.1 M, boehmite is predicted to be heavily agglomerated regardless of the pH. As will be shown later, experimental trends, such as the pH and ionic strength dependence for sedimentation and rheological properties of both boehmite and $Fe(OH)_3$ suspensions, can be rationalized on the basis of such stability diagrams.

2.4 Colloidal Aggregate Fractal Properties

Interparticle potentials not only influence the stability of colloidal suspensions, but are also critical in determining the nature of the agglomerates formed and the kinetics of agglomeration. A critical concept required to understand the nature of agglomerates is that *agglomerates are fractal objects*. For a normal dense solid, the mass of a given particle scales as r^3, where r is the particle radius. For a

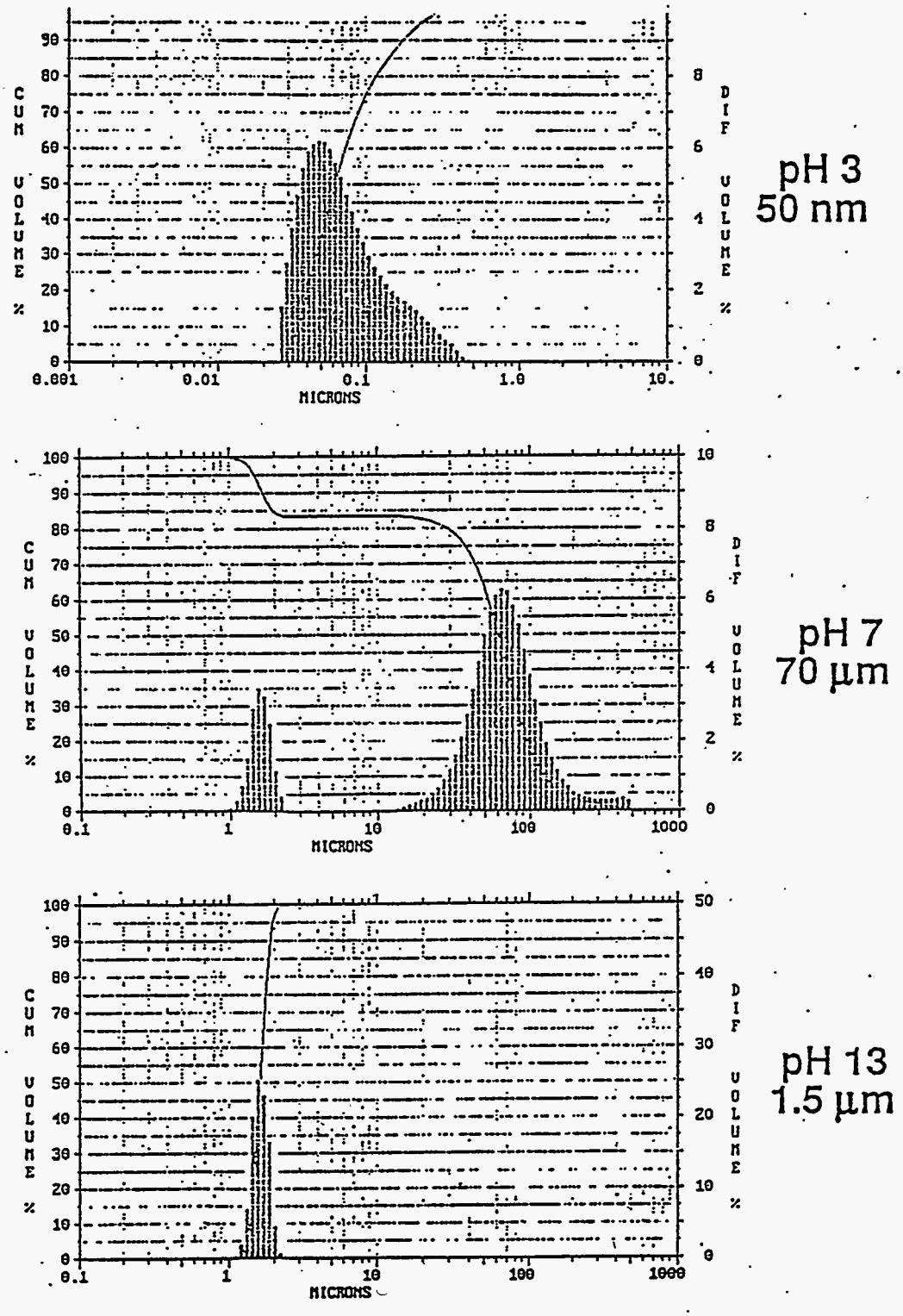

Figure 6. Boehmite (AlOOH) Agglomeration vs. PH. Solids Loading, pH, and Ionic Strength (Salt Content) All Influence Agglomeration

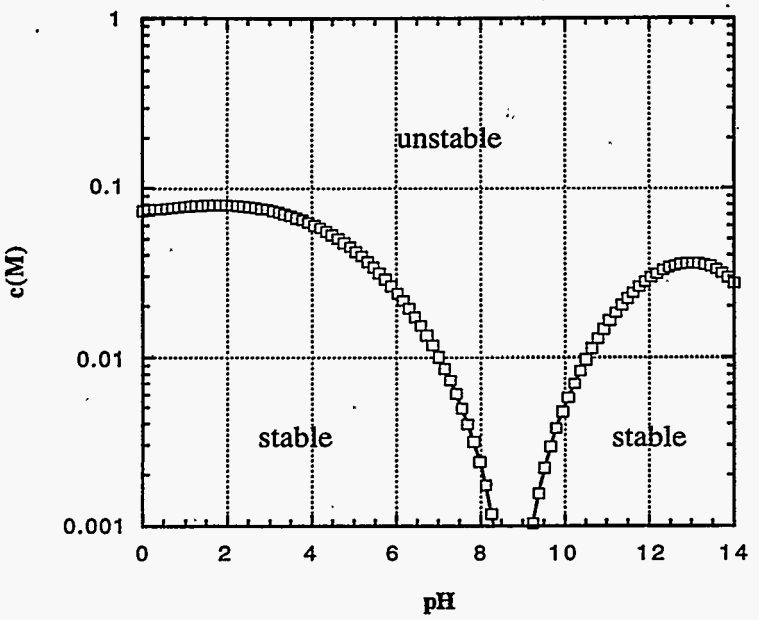

Figure 7. Stability Map for Colloidal Boehmite

fractal three dimensional object, the particle mass scales as r^D, where $D \leq 3$ is called the fractal dimension of the object. The fractal dimension of an agglomerate is controlled by how the agglomerate is formed. For the limiting case of diffusion-limited aggregation, there is no potential energy barrier to agglomeration. Every time a primary particle or cluster encounters another cluster, it sticks. The resulting object tends to have an open network structure with a low density and a low fractal dimension. When there is a significant barrier to agglomeration, particles tend to stick in only those regions of the agglomerate that represent the lowest potential energy sites. In this so-called reaction-limited aggregation regime, denser agglomerates form with a higher fractal dimension. Figure 8 shows images of real fractal agglomerates of 150-nm gold particles formed under the two limiting sets of conditions. Table 2 lists the fractal dimensions for both particle-cluster and cluster-cluster aggregates formed under either diffusion-limited or reaction-limited conditions. For the concentrated slurries representative of sludge, cluster-cluster aggregation is expected and gives rise to limiting fractal dimensions of 1.8 to 2.1 for the diffusion-limited and reaction-limited cases. If the clusters are allowed to rearrange and restructure via rotation around internal points of contact, the clusters can further densify after formation and yield fractal dimensions of 2.18 to 2.25 for the diffusion-limited and reaction-limited cases.

Using the concept of fractals, it is relatively easy to understand the differences between large primary particles and agglomerates made up of small primary particles. First, the density of the fractal object can be much less than that of the primary particle. Conversely, fractal agglomerates occupy much more space than primary particles of the same diameter at equivalent solids loadings.

The density of the fractal object depends both on its size and on its fractal dimension. For example, the $Fe(OH)_3$ we have used in our experimental work contains primary particles that are 10 nm in diameter. If the $Fe(OH)_3$ coagulates to form a relatively dense fractal agglomerate ($D=2.25$) with an average agglomerate diameter of 100 nm, the mass of the agglomerate is only 17.8% that of a

Table 2. Fractal Dimensions of Colloidal Aggregates

		Cluster - Cluster	
	Monomer-Cluster	Polydisperse	Restructered
Diffusion-Limited	2.5	1.8	2.18
Reaction-Limited	3.0	2.1	2.25

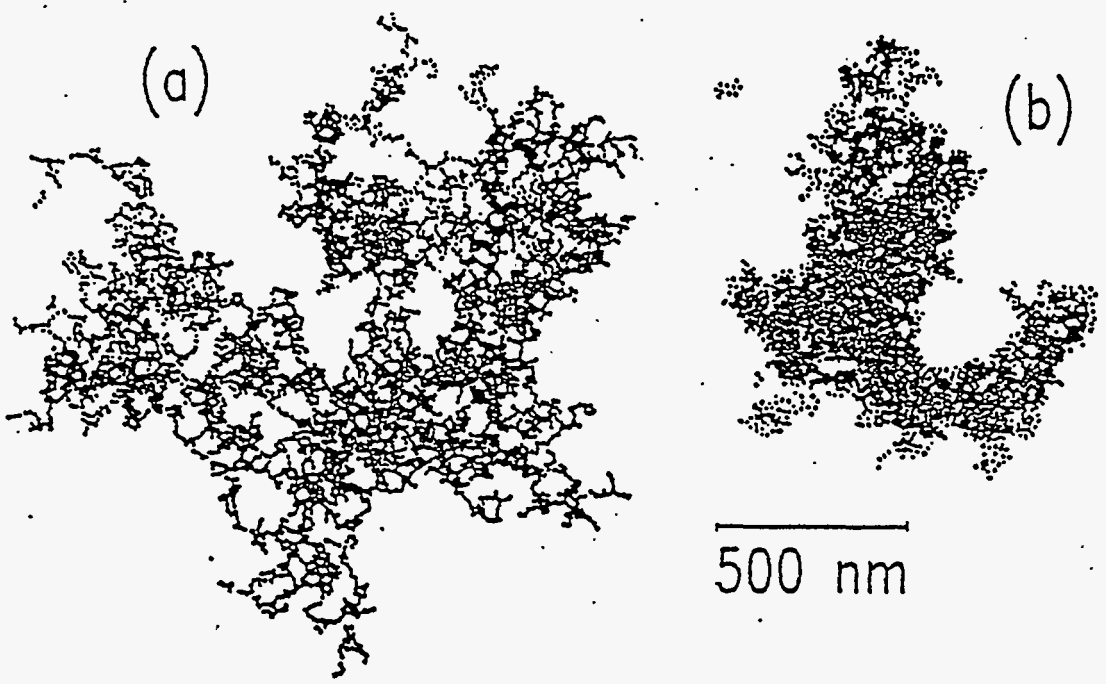

Figure 8. Transmission Electron Micrographs of Clusters Aggregated by Use of (a) Diffusion-Limited Kinetics and (b) Reaction-Limited Kinetics

primary particle having a diameter of 100 nm. For the same fractal dimension, a 1000-nm (1-μm) particle has a net mass that is only 0.56% that of a dense 1-μm primary particle. A 1-mm agglomerate with a lower fractal dimension of D=1.7 would have an even lower relative mass (0.012%).

The aggregation rates used for aggregation kinetics models in Section 2.5 and sedimentation models in Section 3.2 are based on an effective radius, a_k, for each aggregate size k (which indicates the number of primary particles). Colloidal aggregates form fractal structures with a fractal dimension D (where D=3.0 indicates constant packing as a function of radius). The aggregate size k is related to the effective radius by

$$k \sim \left(\frac{a_k}{a}\right)^D \tag{5}$$

where a is the particle radius. The expression for effective aggregate radius becomes

$$a_k = a \left(\frac{k}{\phi_m}\right)^{\frac{1}{D}} \tag{6}$$

where ϕ_m is the maximum packing factor. For spherical particles, ϕ_m=0.64-0.74.

The relative mass of a particle is defined as the mass of the particle minus the mass of an equivalent volume of fluid. The relative density of an aggregate of size k is also calculated using the fractal dimension D by the expression

$$\rho_k = \rho_s \, k^{1-\frac{3}{D}} \phi_m^{\frac{3}{D}} \tag{7}$$

where ρ_s is the relative density of the solid material.

2.5 Aggregation Kinetics

Aggregation kinetics models have been developed to describe the rate of growth of particle aggregates as a function of time. These models are used for systems where the rate of aggregate growth is roughly the same as the rate of sedimentation. These models can also be used to predict the equilibrium aggregate size distribution under different thermal and shear conditions.

If the interparticle interactions have a sufficiently small repulsive barrier, particles or aggregates that collide form a larger aggregate containing k primary particles and having an effective radius a_k (which was discussed in the previous section). For Brownian flocculation, the growth process is controlled by the collision rate between two aggregates (von Smoluchowski 1917)

$$J_{ij} = \frac{2k_B T}{3\mu W_{ij}} (a_i + a_j) \left(\frac{1}{a_i} + \frac{1}{a_j}\right) n_i n_j \tag{8}$$

where n_i and n_j are the corresponding number densities of aggregates containing i and j primary particles, respectively. The stability ratio, W_{ij}, specifies the fraction of collisions between aggregates of sizes i and j that result in having the particles stick to each other to form an aggregate of size i+j. The conservation equation for aggregates of size k can be written as (Sonntag and Strenge 1986)

$$\frac{dn_k}{dt} = \frac{1}{2} \sum_{\substack{i=1 \\ j=k-1}}^{k-1} J_{ij} - \sum_{i=1}^{\infty} J_{ki} \tag{9}$$

where the net change in the number of aggregates of size k is the difference between the first term, which is the rate of increase resulting from collision of smaller aggregates, and the second term, which is the loss resulting from collision with other aggregates to form larger aggregates. A set of these equations for every aggregate size k can be integrated over time to give the aggregate distribution as a function of time.

The stability ratio, W_{ij}, is the ratio of the total number of collisions between aggregates of size i and j to the number of collisions that result in coagulation. Therefore, the stability ratio measures the effectiveness of the potential barrier in preventing the particles from aggregating. For collisions between particles, this ratio is given by the following expression (Sonntag and Strenge 1986):

$$W \equiv \frac{\int_0^\infty \frac{\beta(u)}{(u+2)^2} \exp\left[\frac{V_T(u)}{k_B T}\right] du}{\int_0^\infty \frac{\beta(u)}{(u+2)^2} \exp\left[\frac{V_A(u)}{k_B T}\right] du} \tag{10}$$

where V_T is the DLVO potential energy and V_A is the van der Waals attractive term. The term β represents a hydrodynamic correction factor, which is given by the approximation (Honig, Roebersen, and Wiersema 1971)

$$\beta(u) = \frac{6u^2+13u+2}{6u^2+4u} \tag{11}$$

where u is the separation scaled by the particle radius. The value for the stability ratio depends on the particle types involved and the pH and electrolyte concentration of the solution.

The aggregate size distribution at any point in time is determined by specifying an initial size distribution and then integrating the rate of formation (Equation 9). A computer program has been developed that numerically integrates the rate equations for each aggregate size k. For example, assume an initial distribution consisting only of single particles and a stability ratio $W_{ij}=1$ for all pair combinations. Figure 9 shows the change in relative number densities of aggregates of size k as a function of time. This sample calculation illustrates that once agglomeration begins, monomer concentrations (k=1) rapidly decrease, dimers (k=2) form from monomers, but are eventually destroyed to form trimers (k=3), and other larger cluster sizes also are eventually formed and destroyed. This computational model has been expanded to include aggregate size groups that allow population studies of aggregates with up to 10^{10} primary particles.

For the case where there is no barrier to agglomeration (diffusion-limited aggregation), an equation describing the average agglomerate radius at long times is given by

$$R = (4Ck_BT/3\eta M)^{\frac{1}{D}} t^{\frac{1}{D}} \tag{12}$$

where C is the initial particle concentration, η is the solution viscosity, M is the mass of the primary particle, and D is the fractal dimension. In other words, agglomerates grow faster at higher particle concentrations and when smaller primary particles are present that can diffuse more rapidly. Aggregate growth stops when primary particles are consumed.

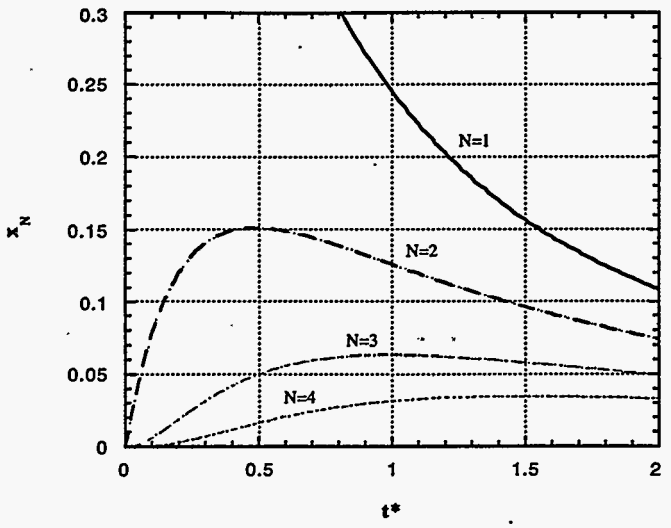

Figure 9. Aggregate Size Distribution as a Function of Time

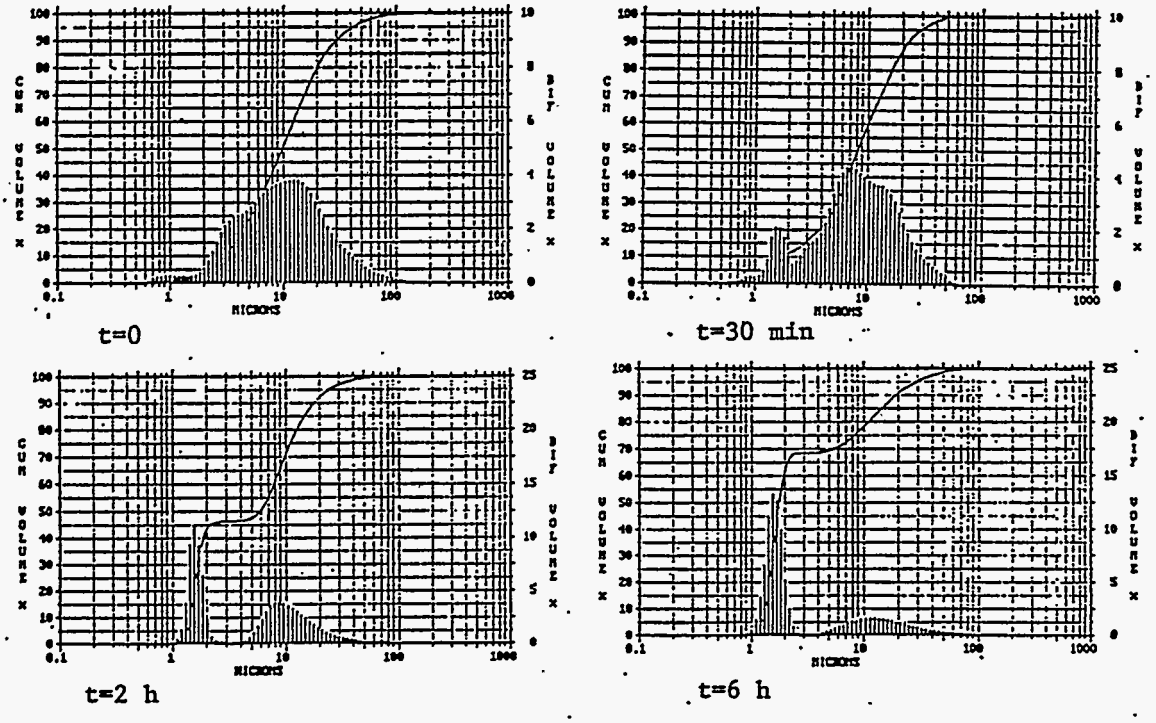

Figure 10. Measured Agglomerate Distributions in Tank C-103 Simulant as a Function of Recirculation Time in the Particle Size Analyzer

Cluster sizes also can be limited by cluster deaggregation, which may occur due to either fluid shear forces or Brownian motion. Literature studies clearly show that high shear rates result in smaller agglomerates. Cluster deaggregation turns out to be a key phenomenon in making agglomerate size measurements. The light-scattering instrumentation used to measure agglomerate sizes requires that the initial concentrated suspensions be diluted to provide the appropriate light- scattering conditions. To keep particles in suspension, the instrument recirculates the solution, so the agglomerates experience shear forces. As a result, the agglomerates deaggregate as a function of time, and the kinetics of deagglomeration can be continuously monitored.

For $Fe(OH)_3$ and a simulant representative of Hanford waste tank C-103, the behavior depicted in Figure 10 is typically observed. Immediately after the suspension is introduced into the instrument, a broad distribution of agglomerates that consist of particles as large as 100 μm and a mean agglomerate size of around 10 μm is observed. However, within half an hour, a new feature appears in the distribution at around 1.6 μm. Over several hours, the large agglomerates continue to disappear until eventually a rather monodisperse agglomerate distribution is produced with a size of 1.6 μm. The above results represent one example of how sensitive "particle size" analyses are to measurement conditions. For most sludge samples, measured particle size distributions are really agglomerate size distributions that are highly sensitive to the concentrations, pH, salt content, and the shear conditions under which the measurements were made. Unless careful attention is given to conditions promoting either agglomeration or deagglomeration, typical "particle size" analyses are relatively meaningless.

Deaggregation terms may be added to the aggregation kinetic model presented in Equation 9. Defining b_{ij} as the rate at which size i+j aggregates break into size i and size j aggregates, the conservation equation for aggregates of size k becomes

$$\frac{dn_k}{dt} = \frac{1}{2}\sum_{\substack{i=1 \\ j=k-1}}^{k-1} J_{ij} - \sum_{i=1}^{\infty} J_{ki} + \sum_{j=1}^{k-1} b_{jk} n_{j+k} - \sum_{j=1}^{k-1} (1+\delta_{j,k-j}) b_{j,k-j} n_k \qquad (13)$$

where δ is the Kronecker delta. By including terms for either shear- or Brownian-induced deaggregation, the equilibrium aggregate size distribution may be calculated by integrating these equations in time to a steady-state solution.

3.0 Effect of Colloidal Aggregation on Sedimentation

Several processing steps during tank waste pretreatment require the separation of solid particles from supernatant liquids using sedimentation processes. In this separation process, a slurry of particles in an aqueous solution generated after transporting, washing, or leaching the sludge is left alone in a storage tank. Over time, the solid particles sink to the bottom under gravity. Ideally, this process yields a dense layer of particles on the bottom of the collection tank with a clear layer of supernatant liquids at the top of the tank. Solid-liquid separation is then readily achieved by merely pumping off the supernatant liquids and leaving the solids behind. Unfortunately, practical experience on both real sludge and on simulants reveals that the "ideal" sedimentation process is often not observed and that many key issues in sedimentation need to be understood and controlled.

Several issues related to the sedimentation process can have a tremendous impact on baseline design. First, the sedimentation velocity must be sufficiently fast (exceeding 3 cm/hr in the current baseline process) to result in a reasonable period of time for each settle-and-decant step. In addition, the final sediment densities influence separation efficiencies by controlling the relative volumes of entrapped interstitial liquids to supernatant liquids that can be removed. Finally, for the treatment of low level waste streams, suspended colloids left in the supernatant liquids after settle-decant operations need to be removed to prevent either contamination or fouling of downstream components such as ion exchangers.

The aggregation of colloidal particles has the potential for significantly impacting each of these issues. For example, Table 3 shows the effect of varying the primary particle size, agglomerate diameter, and fractal dimension of the agglomerate on two important sedimentation parameters: the gel point and settling rate. The table is based on 50-nm diameter primary particles with a specific density four times that of water.

The settling rate is defined by the primary particle size, agglomerate diameter, and fractal dimension of the agglomerate. For the same primary particle size (0.01 μm) and fractal dimension (2.5), increasing the agglomerate diameter results in an increased settling rate, a trend that is similar to that for solid spherical particles. For the same agglomerate diameter (100 μm) and fractal dimension (1.8, 2.5), increasing the primary particle size increases the solids density of the agglomerate resulting in an increased settling rate. Finally, increasing the fractal dimension at constant primary particle and agglomerate sizes results in an increased settling rate. It is important to note that agglomerates that have the same size do not necessarily settle at the same rate. Therefore, primary particle size, fractal dimension, and agglomerate size must all be known to predict the settling behavior of colloidal suspensions.

The gel point is defined as the volume fraction at which the agglomerates become interconnected to form a network. The gel point controls the extent to which the sediment bed will pack, and therefore controls the final sediment bed density. The trends are similar to those for the settling rate. Note that an increased primary particle size or increased fractal dimension results in a higher solids density and, therefore, a higher gel point.

Table 3. Dependence of Sedimentation Parameters on Agglomerate Properties

Primary Diameter	Agglomerate Diameter	Fractal Dimension	Gel Point (vol%)	Settling Rate (cm/hr)
0.01 μm	100 μm	1.8	0.32%	0.07
1 μm	100 μm	1.8	2.7%	18
0.01 μm	100 μm	2.5	3%	72
1 μm	100 μm	2.5	10%	3000
0.01 μm	1 μm	2.5	10%	0.036
0.01 μm	10 μm	2.5	7%	1.4
0.01 μm	100 μm	2.5	3%	72
100 μm	100 μm	3.0	16%	6000

The impact of sediment cake densities on settle-decant steps is illustrated in Figure 11. In an ideal settle-decant step, all particles would sink to the bottom after mixing to form a highly compact solid mass containing little interstitial liquid. For a slurry with 10 vol% solids loading, sedimentation of monodisperse spheres could form a solid layer filling only 14% of the tank volume, in which 74 vol% of the material in the layer is particles and 26 vol% is interstitial liquid. Of the total liquid in the tank, 96% would be supernatant liquid that could be removed by pumping, while only 4% to the total liquid would remain as interstitial liquid. For such a system, solid-liquid separations via settle-decant processing is highly efficient. However, if final sediment densities are 25 to 30 vol% as seen experimentally, then the final sediment can occupy roughly half of the total tank volume and contain roughly 1/3 of the total liquid present in the tank. For this case, the solid-liquid separation step can only remove 2/3 of the tank liquids, leading to an inefficient separation. In extreme cases, where the suspended particles form a gel, there are no supernatant liquids, and there can be no solid-liquid separations. Therefore, the extent and fractal nature of colloidal agglomeration is critical to an evaluation of settle-decant steps.

In Section 3.1, we describe the experimentally observed sedimentation behavior of both model colloidal systems and actual tank sludge. Sections 3.2 and 3.3 describe the sedimentation models that have been developed to describe this behavior. Section 3.4 provides an example of how these models are used to predict the sedimentation behavior of a colloidal system.

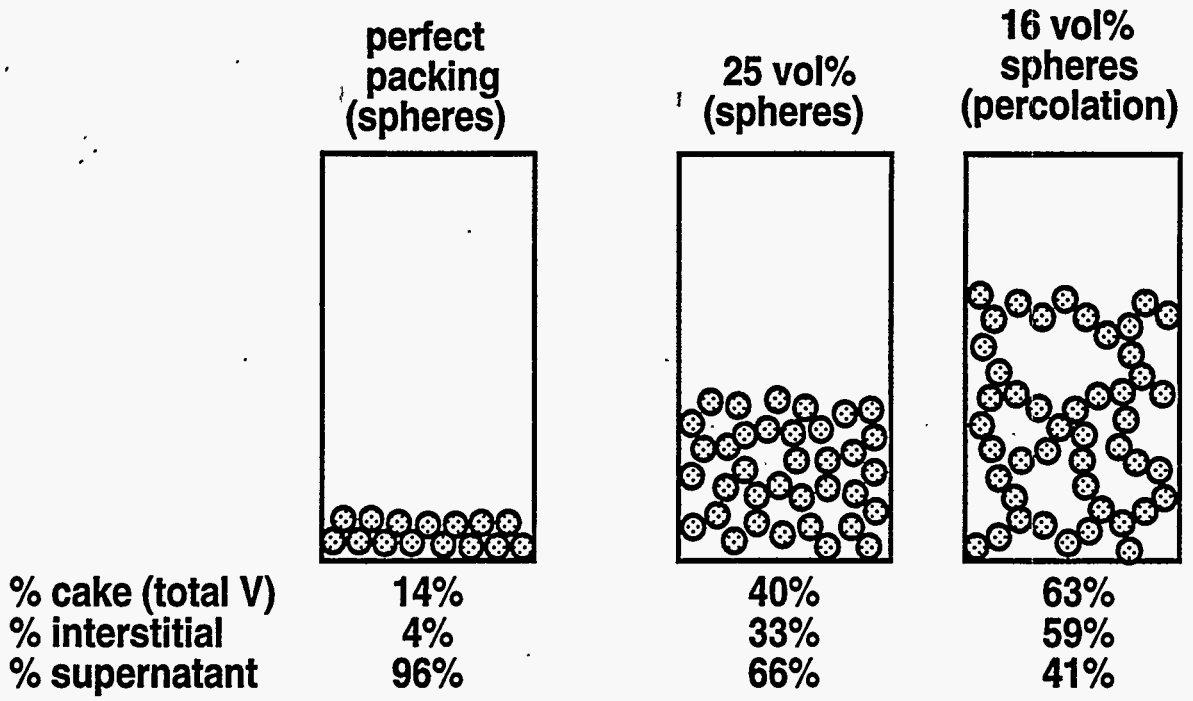

Figure 11. Impact of Agglomeration on Settle-Decant Steps. Example: 10 vol% slurry.

3.1 Sedimentation Behavior of Colloidal Systems

A series of sedimentation experiments were performed for a variety of colloidal suspensions, including 0.25-, 1-, and 10-μm particles of gibbsite, 50-nm x 5-nm boehmite plates, 5-10 nm particles of $Fe(OH)_3$, and multicomponent simulants for Tank C-103 sludge. The sedimentation velocities for each suspension were measured by pouring the suspensions into clear cylinders and then watching the position of the boundary between the clear supernatant liquid and the settling sediment as a function of time.

The general characteristics observed during sedimentation are illustrated in Figure 12 using $Fe(OH)_3$ suspensions in pH 12 water with different initial solids loadings. For samples with a relatively high solids loading (at or above 4 wt% in this case), a sharp, well-defined interface appears almost immediately between clear supernatant liquid and an opaque region that contains suspended solids. For such suspensions, the sedimentation velocity is monitored by noting the position of the interface as a function of time. With time, the sediment layer becomes thinner as the sediment settles. The average solids loading in the sediment layer increases until the sediment compresses to its equilibrium solids loading profile. For samples with low solids loadings (below 4 wt%), three separate regions appear: a clear supernatant liquid, an opaque region that contains suspended solids, and a concentrated sediment layer. For some samples with an extremely low solids loading, the interface between the supernatant liquid and sedimenting particle region is not sharply defined. Over time, the sediment layer is observed growing up from the bottom of the container. The layer gets thicker with time (in contrast to the behavior of concentrated suspensions) as particles settle to the bottom.

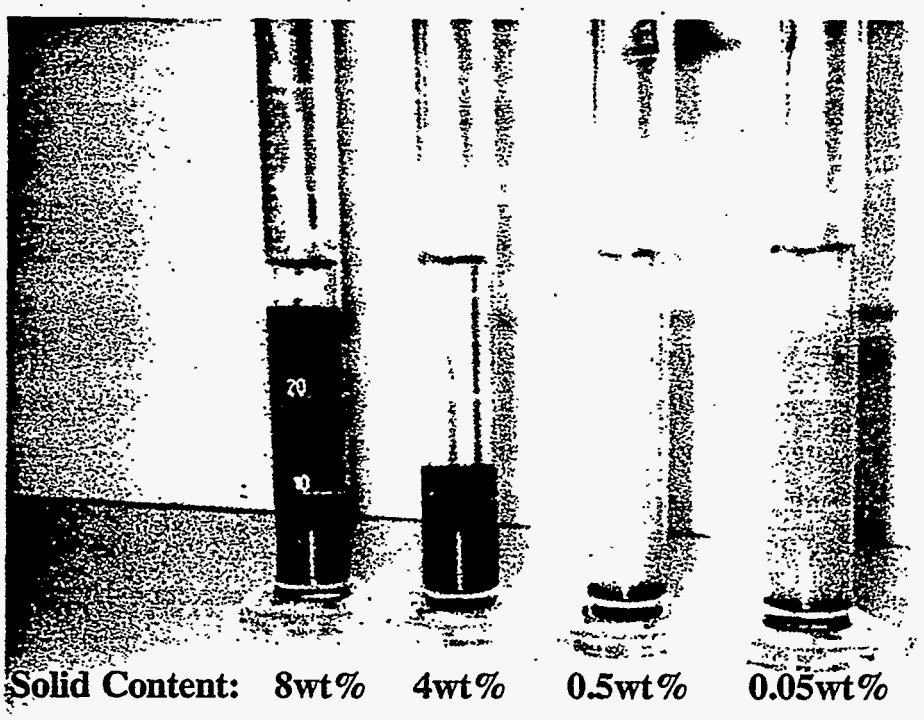

Figure 12. Sedimentation Behavior of $Fe(OH)_3$ Suspensions at Different Solids Loadings

The difference between the sedimentation behavior of the high and low solids loadings cases can be explained by understanding the behavior of the agglomerates in suspension. For very low solids loadings, particle agglomerates form and settle as individual particles. As the initial solids loading increases, the agglomerates are concentrated enough to hydrodynamically interfere with each other so as to cause hindered settling, similar to what occurs with solid particles except at much lower solids loadings. However, the agglomerates are still free to fall until they reach the bottom of the container, where they begin to form a sediment layer.

When the initial solids volume fraction exceeds a specific value, known as the gel point, ϕ_g, the agglomerates form a network and the suspension takes on the form of a solid structure. Compressive stresses on the system can be transmitted via the network and the structure then possesses the ability to at least partially support itself. In this case, the rate of compression of the sediment is controlled by a combination of the hydrodynamic drag of the interstitial fluid being squeezed out of the network and the breaking and reforming of particle bonds as the agglomerates are being crushed by the weight of the sediment above.

It is essential that we evaluate how the behavior displayed in these simple experimental systems represents the behavior of actual tank sludges. Recently, sedimentation data on sludge from Tanks S-104, T-111, BX-107, T-104, and B-111 have been obtained in the laboratory. The objective of these experiments was to investigate how these sludges behave under standard washing and leaching procedures. Solutions used in the sedimentation studies correspond to retrieval wash (2.3 wt% solids in 0.01 M NaOH and $NaNO_3$ at 100°C for one hour), caustic leaching (8 wt% solids in 3 M NaOH at

100°C for 5 hours), and final washing (8 wt% solids in 0.01 M NaOH and $NaNO_3$ at 25°C for half an hour). While details of their results are described elsewhere (Rapko, Lumetta, and Wagner 1995), we have analyzed their results in the context of the results obtained on the simple systems described earlier.

The sedimentation results obtained at 8 wt% solids loadings (for the caustic leach and final wash) are indicative of hindered settling above the gel point for all sludges examined to date. No sedimentation is observed at all for Tank B-111, T-111, and S-104 sludges, while Tank T-104 and BX-107 sludges exhibit slight compaction. At 2.3 wt% (retrieval wash conditions), significant sedimentation is observed for all samples. Observed initial sedimentation velocities range from a maximum of 3.2 cm/hr for T-104 sludge to a minimum of 0.2 cm/hr for S-104 sludge. Final average sediment densities range from 3.4 wt% for S-104 to 12 wt% for T-104.

It is interesting to compare the sedimentation results observed for actual tank sludges with the behavior of simple simulants. TEM and elemental analyses show that Tank S-104 sludge consists largely of boehmite. The primary particle size of the boehmite is around 0.1 μm, which is only twice as large as the 0.05-μm particles found for the commercial boehmite used in our sedimentation studies. In terms of final sediment density, S-104 sludge is comparable to boehmite under similar sedimentation conditions (3.4 wt% for S-104 compared with 2.9 wt% for commercial boehmite). The slight increase in sediment density for S-104 sludge is consistent with the slightly larger primary particle size. In terms of sedimentation rate, 2 wt% commercial boehmite settles at a rate of around 0.5 cm/hr compared with 0.2 cm/hr for S-104. Again, the lab tests on single component boehmite come close to replicating the behavior of tank sludges that contain similar particles.

TEM results show that Tanks T-111 and B-111 contain sludges consisting primarily of the bismuth-iron-silicate phase. High resolution images suggest that this phase closely resembles commercial $Fe(OH)_3$ both in terms of its primary particle (sub-μm) and agglomerate distributions. Sediment densities for T-111 and B-111 sludges in lab-scale tests of 6.2 wt% and 5.9 wt%, respectively, are close to the equilibrium sediment densities measured for $Fe(OH)_3$ of 6.7 wt%. Initial sedimentation velocities of 2.8 and 1.2 cm/hr for T-111 and B-111 sludges, respectively, are comparable to the value of around 2 cm/hr measured for $Fe(OH)_3$ at 2 wt% solids.

3.2 Compressive Yield Stress

A computational model has been developed that describes the density due to compression of the sediment layer at any vertical position resulting from the weight of the sediment above it. This model can be used to predict the equilibrium sediment density profile and sediment height for a particular suspension given the total initial solids loading. This model is also part of the transient sedimentation model described in the next section.

As discussed in the previous section, when the particle volume fraction is sufficiently high, a network of connected aggregates forms and the suspension takes on the form of a solid structure. In particular, compressive stresses on the system can be transmitted via the network throughout the system and the structure then possesses the ability to support itself. When such a network has formed, a pressure can be applied either mechanically, such as with a piston, or through gravitational forces. As the pressure is increased, the network structure will resist further compression until the forces become

so strong that the structure will begin to deform irreversibly. The rheological property to describe this is the compressive yield stress, $P_y(\phi)$, which is defined as the value of the network pressure at which the flocculated suspension at volume fraction ϕ will no longer resist compression elastically, and will start to yield and so irreversibly consolidate. A simple definition of the compressive yield stress at any vertical location is the relative weight of the sediment above that location. It is calculated by multiplying the integral of the volume fraction by the difference between the solid and liquid densities.

The compressive yield stress, $P_y(\phi)$, is an implicit function of many variables, including the size, shape, composition and the relative number of particles involved, and the interparticle forces (which in turn depends on the solution chemistry). The form of the dependence of $P_y(\phi)$ on the volume fraction is illustrated in Figure 13 for a system with $Fe(OH)_3$ particles in a solution of water with pH 12. This form can be divided into two regions, with the boundary defined by the gel point volume fraction, ϕ_g. The gel point for this system is approximately 1.0 vol%. Below this value, the aggregates are not connected and act as independent units. At the gel point, these aggregates become interconnected throughout the container to the extent that they are able to support a load. Above the gel point, the compressive yield stress is typically modeled using power law curves of the following type (Landman, White, and Buscall 1988):

$$P_y(\phi) = c\left[\left(\frac{\phi}{\phi_g}\right) - 1\right]^m \qquad \phi>\phi_g \tag{14a}$$

or

$$P_y(\phi) = c\left[\left(\frac{\phi}{\phi_g}\right)^n - 1\right] \qquad \phi>\phi_g \tag{14b}$$

With m varying between 4 and 10 and n varying between 8 and 10. These curves have been fitted to experimental systems such as polystyrene latex (Buscall et al. 1987) and red mud suspensions (DeGuingand 1986).

The parameters for the power law curves may be determined using equilibrium sediment height data. The only information required is the solid and liquid densities, the weight or volume percent of particulate solids, and the final sediment height. Data for at least three different sediment heights are required. A computer program has been written to optimize the power law parameters (c, ϕ_g, and n or m) by performing a least-squares fit based on the sediment heights using a simulated annealing approach. The exponents are restricted to the ranges specified above.

As an example, the results of this model for a system with $Fe(OH)_3$ particles in a solution of water with pH 12 and zero ionic strength are shown in Figures 13-15. A series of sedimentation experiments were performed by filling 10-cm-high cylinders with 0.5, 1.0, 2.0, 4.0 and 8.0 wt% suspensions of $Fe(OH)_3$ particles in water. After the particles settled, the height of the sediment bed was measured. The parameters for Equation 14a were determined by performing a least-squares fit on the data. The compressive yield stress as a function of volume fraction is shown in Figure 13. The sediment height for a given solids loading is determined by integrating this curve until the total relative weight of the solids is achieved. A comparison of the experimental results with the calculated sediment heights for each sedimentation experiment is shown in Figure 14. The sediment density profile as a function of distance from the top of the sediment layer is presented in Figure 15.

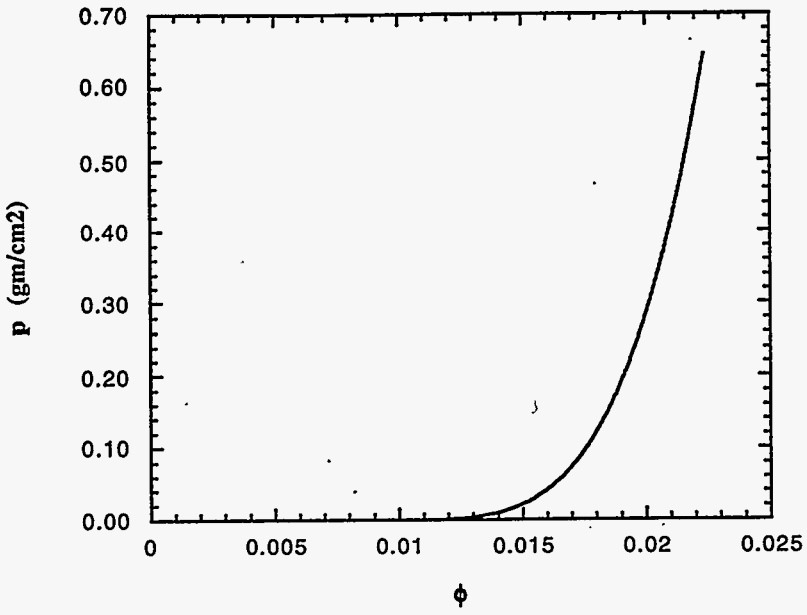

Figure 13. Compressive Yield Stress vs. Volume Fraction ($Fe(OH)_3$ in pH12 water)

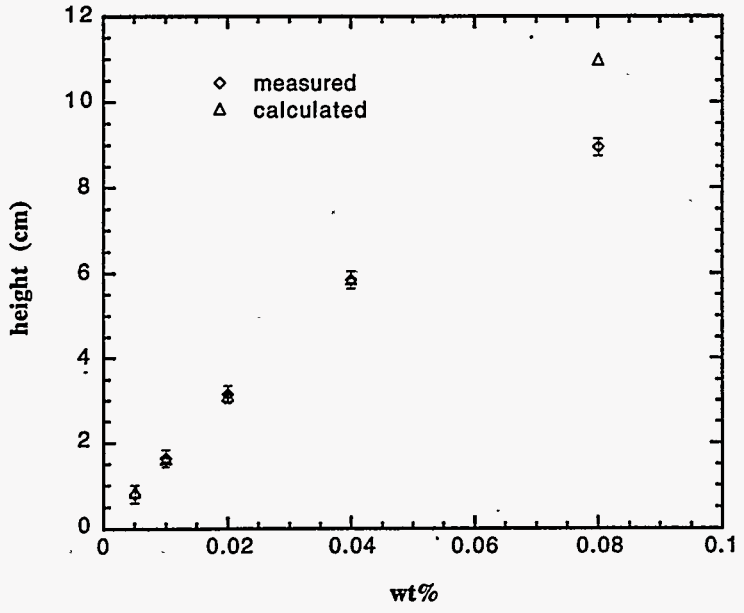

Figure 14. Measured and Calculated Sediment Heights ($Fe(OH)_3$ in pH12 water)

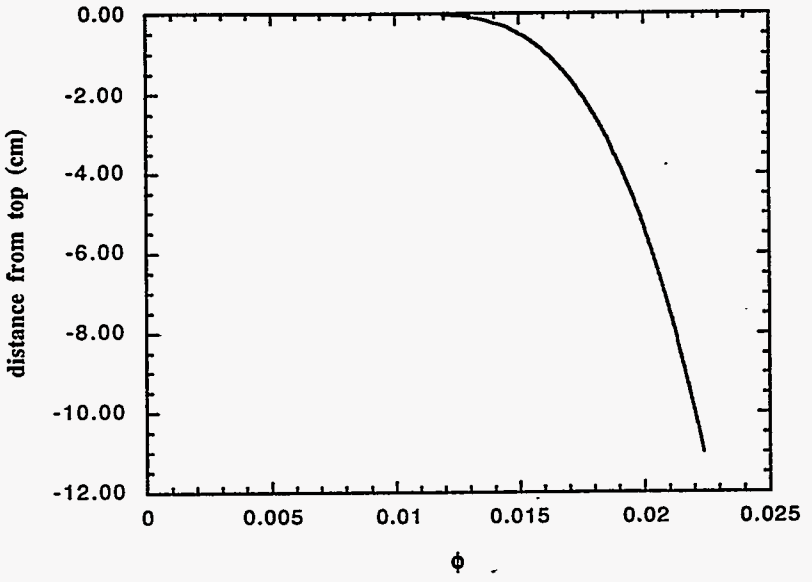

Figure 15. Sediment Density Profile vs. Distance From the Top of the Sediment Layer ($Fe(OH)_3$ in pH12 water)

Note the discrepancy between the measured and calculated sediment heights in the 8.0-wt% case. This is due to the fact that the initial solids loading at the beginning of the experiment was approximately 2.0 vol%, which is significantly greater than the gel point of 1.0 vol%. Therefore, the top of the sediment density profiles (Figure 15) was "crushed" to 2.0 vol% and remained at that density as the rest of the layer compressed. However, if additional water was added to increase the column height above 10 cm and the sediment was resuspended, the final sediment height would be approximately 11 cm as shown in Figure 13. This helps to explain the observation that stirring and adding water to a sediment can sometimes result in a dramatic increase in apparent sediment volume.

Using the procedure described above, empirical power law curves were calculated for a variety of systems using equilibrium sediment height data. The resulting parameters are shown in Table 4. The parameters ϕ_g and m define the shape of the curve and the parameter c controls the magnitude.

By examining the parameter values for different systems, we notice certain trends. In Table 2, we noted that the fractal dimension of diffusion-limited aggregate was less than that for a reaction-limited aggregate. As the ionic concentration of the solution is increased, the particle-particle reaction barriers are reduced, resulting in diffusion-limited aggregation. The lower fractal dimension results in a lower density aggregate, which translates into a lower gel point. However, the lower sediment density also means that the sediment is more "crushable," and the scaling parameter, c, decreases with increasing ionic concentration.

In Table 3 we noted that a larger primary particle diameter for the same fractal dimension resulted in a significantly higher gel point. The gibbsite particles have a particle diameter on the order of

Table 4. Parameters for Compressive Yield Stress Model

System	ϕ_g	c	m
$Fe(OH)_3$, pH 12, water	0.009564	0.2012	4
$Fe(OH)_3$, pH 12, 0.25M $NaNO_3$	0.008672	0.1668	4
$Fe(OH)_3$, pH 12, 1.0M $NaNO_3$	0.006401	0.01167	4
Gibbsite S-3, 0.1M $NaOH_3$	0.06768	164.0	4

0.25-μm as compared with 50-nm x 5-nm boehmite plates. The difference in particle size results in an order of magnitude increase in the gel point. The higher sediment density also results in an increase in the compressive yield scaling factor.

3.3 Transient Sedimentation Model

A computational transient sedimentation model has been developed to predict the settling behavior of these colloidal aggregates in tank wastes. This sedimentation model consists of three primary features: a compressive yield stress model, a hindered settling model, and an aggregation model. The compressive yield stress (described in the previous section) relates the weight of the overlying sediment to the density of the sediment at any axial position and can typically be described by a power law expression. Once the functional form for the compressive yield stress has been established for a particular particulate system, the equilibrium sediment height and density profile can be predicted given the total solids loading. The hindered settling model predicts the rate of settling for particulate aggregates based on the primary particle size, total aggregate size, and fractal dimension. The model may be applied to an equilibrium aggregate size or a range of developing aggregates, if the time scale of aggregation is similar to that of sedimentation. If this is true, the kinetic aggregation model (described in Section 2.5) may be used to calculate the change in aggregate distribution as a function of time. Above the gel point, a dynamic compression factor describes the rate of sediment compression. The basic equations used in this model were developed by Buscall and White (1987).

The sedimentation model divides the system into two regions. In the upper region, the solids concentration is below the gel point, ϕ_g, for that suspension and the particle agglomerates interact only through hydrodynamic forces. In this region, the velocities of the agglomerates in this region are given by the expression

$$u = \frac{u_0(1-\phi)}{r(\phi)} \tag{15}$$

where u_0 is the Stokes settling velocity at infinite dilution and $r(\phi)$ is a dimensionless hydrodynamic interaction parameter. The term $(1-\phi)$ results from the fact that the volume displacement of downward flowing solids must be compensated by an equal upward volume flow of solution. The term converts the relative velocity of solids to solution into an reference frame velocity. The Stokes settling velocity, u_0, for solid spherical particles is given by the expression

$$u_0 = \frac{2a^2\Delta\rho g}{9\eta_s} \tag{16}$$

where a is the particle radius, $\Delta\rho$ is the solid-liquid density difference, and η_s is the solution viscosity. For particle agglomerates containing k primary particles, the radius becomes the effective agglomerate radius, a_k, defined by Equation 6 and the density is given by the relative density, ρ_k, defined by Equation 7.

The hydrodynamic interaction parameter, $r(\phi)$, can take many forms, but the most common is the expression

$$r(\phi) = (1 - \frac{\phi}{\phi_{ref}})^n \tag{17}$$

where ϕ_{ref} is a reference volume fraction. For solid spherical particles with no interactions, ϕ_{ref} is usually set equal to one or the close-packed volume fraction $\phi_{cp}=0.64$ and the exponent n is between -4.5 and -5.5. For particle agglomerates, the value for ϕ_{ref} is related to the gel point for that system.

In the lower region, the solids concentration is above the gel point, ϕ_g, and the particle agglomerates interact through both hydrodynamic forces, represented by $r(\phi)$, and solid network stresses. The velocities of the agglomerates in this region are given by the expression

$$u = \frac{u_0(1-\phi)}{r(\phi)}(1 + \frac{\partial P/\partial z}{(\Delta\rho g\phi)}) \tag{18}$$

where P is the network stress at elevation z, and the term $\Delta\rho g\phi$ is the change in gravitational head per unit elevation. Note that for regions where there is no network stress, the last term is zero and the expression reduces to Equation 15. For sediments that have reached equilibrium, the change in network stress is equal to negative the change in gravitational head, resulting in a net velocity of zero.

In Section 3.2, we described the compressive yield stress, $P_y(\phi)$, of a suspension. If the network stress, P, is less than or equal to the compressive yield stress, the network is strong enough to support the weight of the sediment and no change occurs. However, when the network stress exceeds the compressive yield stress, the network consolidates irreversibly until the volume fraction, ϕ, increases to the point where the yield stress equals the network stress. The rate at which this change occurs is controlled by the dynamic compressibility, $k(\phi)$. The network velocity is controlled by the expression

$$\frac{\partial u}{\partial z} = \frac{\kappa(\phi)}{\phi}[P - P_y(\phi)]; \qquad P \geq P_y(\phi) \tag{19}$$

$$= 0; \qquad P < P_y(\phi)$$

When Equation 18 is substituted into this expression, we obtain a second-order differential equation for the network stress

$$\frac{\partial}{\partial z}\left[\frac{(1-\phi)}{r(\phi)}(1 + \frac{\partial P/\partial z}{(\Delta\rho g\phi)})\right] = \frac{\kappa(\phi)}{u_0}[P - P_y(\phi)] \tag{20}$$

where the right-hand term is zero when $P < P_y(\phi)$.

A computational model has been developed that combines the hindered settling model, the network stress model, and the aggregation kinetics model (when appropriate) to predict the sedimentation behavior of suspensions. Both time and elevation are discretized using a finite-difference formulation. The following procedure is followed for each time step:

- The total solids volume fraction, ϕ, is calculated at each elevation by summing the solids volume fraction for each agglomerate size, ϕ_k. If the total solids volume fraction exceeds the gel point ($\phi > \phi_g$), the node is considered part of the sediment layer. The elevation node that represents the top of the sediment layer is located. This divides the system into two regions.

- In the upper region, the agglomerate velocities are calculated for each agglomerate size, k, using a hydrodynamic interaction factor based on the local agglomerate concentration. The velocities are used to calculate solids transport from one elevation to another using an upwind-differencing formulation. Because this term is explicit in time, the time step, Dt, is restricted by the Courant limit (Andersen, Tannehill, and Pletcher 1984)

$$\Delta t = \frac{\Delta x}{u_k} \tag{21}$$

- In the lower region, the network stress is calculated using Equation 20. The network stress at the top of the sediment layer is assumed to be zero. The network stresses are then used to calculate the sediment velocity at each elevation using Equation 18, which is then used to calculate solids transport for that time step.

- If the aggregation time scale is on the same order as that for sedimentation, the aggregation kinetics model is used to calculate the change in the aggregate size distribution at each axial level using Equation 13. If the aggregation time scale is much smaller, an equilibrium aggregate size distribution is assumed.

The unknown parameters that must be defined in order to use this model for any particular suspension are the compressive yield stress, $P_y(\phi)$, the hydrodynamic interaction parameter, $r(\phi)$, and the dynamic compressibility, $k(\phi)$. The compressive yield stress curve may be determined using equilibrium sedimentation data for different total solids content as described in the previous section. The hydrodynamic interaction parameter may be fitted using transient sedimentation data at different initial solids concentrations. The dynamic compressibility may also be fitted using these data. Experience has shown that the sedimentation behavior is relatively insensitive to the form used for the dynamic compressibility and becomes noticeable only in the final stages of sediment compression.

3.4 Comparison with Experimental Data

Once the compressive yield stress, hydrodynamic interaction parameter and dynamic compressibility have been established for a particular system, both the equilibrium sedimentation height and transient sedimentation behavior can be predicted for a wide range of column heights and solids loadings. For example, Figure 16 shows the predicted sediment heights for different solids loading of $Fe(OH)_3$ in pH 12 water. The compressive yield stress curve for this system is presented in Figure 13. The gel point is approximately 1.0 vol% or just under 4.0 wt%.

The data points in Figure 16 are the change in elevation of the interface between the clear supernatant liquid and the settling suspension. The suspensions with an initial solid volume fraction that is above the gel point (4 and 8 wt%) have only one interface and the calculated curves shown are the elevations at which the volume fraction equals the gel point. The suspensions with an initial solid volume fraction that is less than the gel point (1 and 2 wt%) have two interfaces, one between the clear supernatant and the falling suspension and one between the suspension and a sediment layer, growing from the bottom of the container. The calculated curves shown represent the location of the upper interface and are based on the elevation for half the initial concentration.

This information can then be extrapolated to predict the behavior of production systems. Figure 17 shows the sedimentation curve calculated for a 4 wt% $Fe(OH)_3$ suspension in a settling tank with an initial sediment height of 10 m. The calculations indicate that sediment levels should drop by 2 meters in one month and that complete settling could take over three months. The average final density of the sediment layer will be approximately three times that of the initial solids volume fraction, or around 12 wt%. Note that this solids loading is higher than that achieved in small lab-scale experiments due to the added weight of the taller sediment column.

This example demonstrates the immediate usefulness of this computational model, that of extrapolating benchtop experimental data to predict the sedimentation behavior of engineering systems. The compressive yield stress curve is obtained from a series of equilibrium sediment height data. The hydrodynamic interaction parameter and dynamic compressibility are obtained from transient sedimentation data. Once these have been established, the sedimentation behavior for a system of any height or concentration can be predicted. As more is understood about the relationship of these functions and the physical structure of the colloidal agglomerates and gel network, the more we will be able to predict these functions *a priori*.

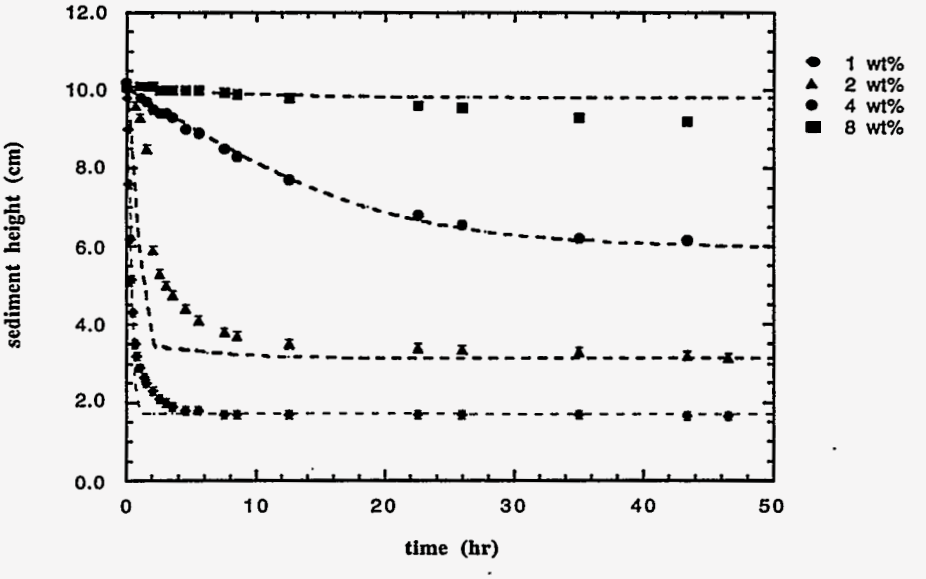

Figure 16. Comparison of Predicted and Measured Sediment Heights for Various Solids Loading of $Fe(OH)_3$ in pH12 Water

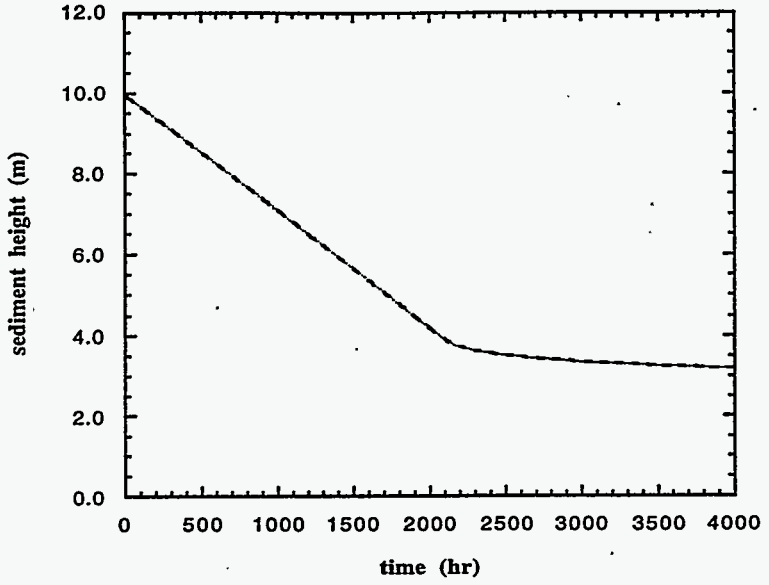

Figure 17. Predicted Sedimentation Curve for a 4 wt% $Fe(OH)_3$ Suspension in a Settling Tank with an Initial Sediment Height of 10 m

4.0 Effect of Colloidal Aggregation on Suspension Rheology

The processing of Hanford tank waste requires the retrieval and transport of the waste from the tanks before pretreatment. The main processing goal is to be able to produce low viscosity solutions (< 60 cP) having the highest possible loadings of suspended particles. Low viscosity suspensions are required to ensure that fluids can be pumped and that transfer lines are not plugged. High solids loadings are required to minimize the volume of waste to be treated. Experience has shown that some suspensions with solids loadings of over 10 vol% can meet these criteria. However, other suspensions with less than 3 vol% solids loading can form a gel that can exhibit viscosities greater than 25,000 cP. The rheological properties of these suspensions appear to depend not only on the particles in the suspension but also on the solution chemistry.

The purpose of this work is to understand the effect of colloidal aggregation on suspension rheology. We can then use this information to predict the rheological behavior of tank waste at different stages of retrieval, transport, and pretreatment. The approach we have taken is to measure the rheological properties of simple single component suspensions under a variety of conditions. Computational models are then developed to provide a framework for understanding the trends in the results. These models can then be used to predict the properties of similar systems. Once this has been accomplished, the methodology can be extended to both simple and complex mixtures of particle types.

To evaluate whether the goal of low viscosity, high solids loading sludges can be produced, experimental studies have been performed to determine the viscosity behavior of individual sludge components. The results of these studies are presented in Section 4.1. The discrete and empirical computational models that have been developed to understand the rheological properties of suspensions are described in Section 4.2. The application of these models to experimental data is described in Section 4.3.

4.1 Rheological Behavior of Colloidal Systems

Viscosity studies were conducted on a variety of suspensions as a function of solids loading, pH, and ionic strength. Suspensions that were examined include boehmite (AlOOH), gibbsite [$Al(OH)_3$], and iron hydroxide [$Fe(OH)_3$]. The purpose of these studies was to establish the range of behaviors that might be encountered for suspensions that contain submicron primary particles.

The viscosity of colloidal suspensions depend on the size, shape, solids loading, and interactions between particles. For perfectly spherical, non-interacting particles, theoretical calculations (see Section 4.2) predict that the viscosity should increase with solids loading, but that viscosities should stay below 50 cP even at solids loadings as high as 50 vol%. For boehmite in a 0.01 M $NaNO_3$ solution, individual primary particles are non-interacting and are not agglomerated at pH 3. Viscosity measurements on boehmite suspensions at pH 3 (Figure 18) are consistent with the behavior predicted for non-interacting particles. Suspensions with up to at least 10 vol% solids loading have low viscosities (< 5 cP) and behave like Newtonian liquids (i.e., the viscosity is independent of shear rate). Such suspensions of non-agglomerated particles would be well suited for transport during waste processing.

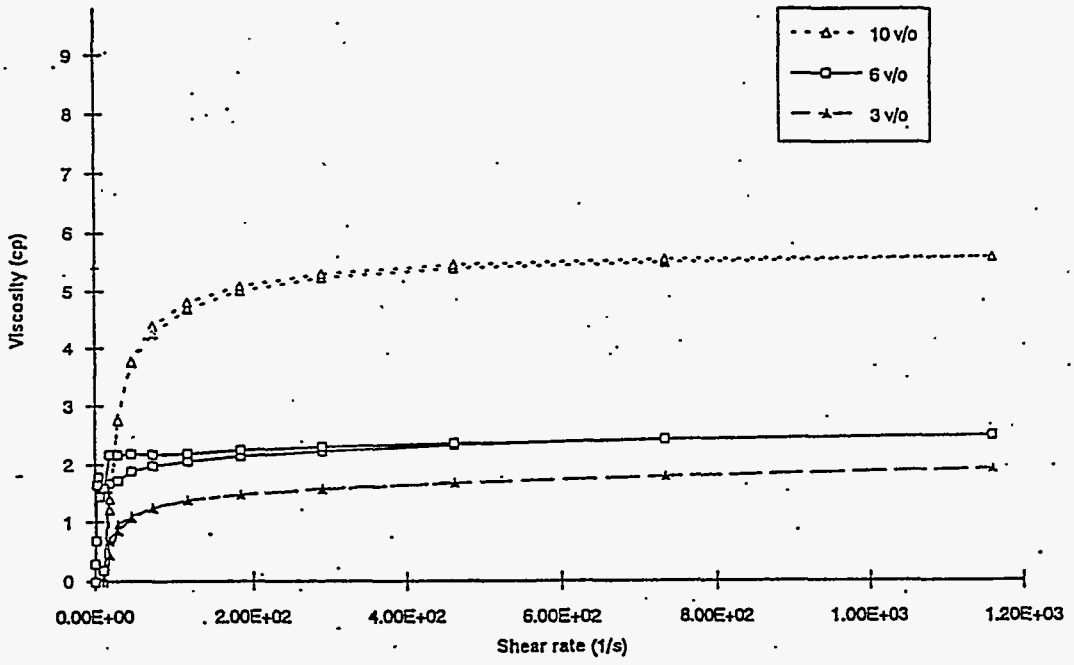

Figure 18. Effective Viscosity of Dispersed Boehmite Suspensions in a pH3, 0.01 M $NaNO_3$ Solution (stirred for 2 hours)

The viscosity behavior of agglomerated boehmite suspensions is in sharp contrast to the behavior observed at pH 3. For example, at pH 10 (Figure 19), the viscosity of a 10 vol% suspension exceeds 10,000 cP at low shear rates (below 20 s^{-1}). The agglomerated slurries are non-Newtonian shear-thinning liquids. Note that the viscosity dramatically increases with solids loading.

The rheological behavior of colloidal suspensions is determined to a large extent by the formation of aggregates or gel networks by the colloidal particles. For very low particle concentrations in a shearing fluid, the particles form aggregates that move independently of each other. The suspensions behave like a Newtonian fluid. As the concentration increases, the aggregates interfere with each other and increase the resistance of the suspension to shear. When the solids concentration exceeds the gel point, the suspension attempts to form a gel network of interconnecting aggregates. For very low shear rates, particle-particle bonds within the network are broken but then quickly form new bonds. The gel has properties much like an elastic solid. As the shear rate is increased, fewer bonds have the chance to reform. At very high shear rates, the gel network structure is totally disrupted and the suspension behaves like a fluid with a high solids loading.

The effect of pH and ionic strength on slurry viscosity is illustrated in Figure 20 for boehmite samples with 10^{-2} M $NaNO_3$ at a shear rate of 11.5 s^{-1}. The solid points represent experimental data and the curves represent behavior expected for the suspensions. The viscosity measurements indicate that while the viscosity values follow the general trends indicated in the boehmite stability diagram (Figure 7), the value of kT that defines the stability curve is probably set too low. A value of around 4 kT comes close to describing the observed viscosity behavior and indicates slight agglomeration in the basic pH regime.

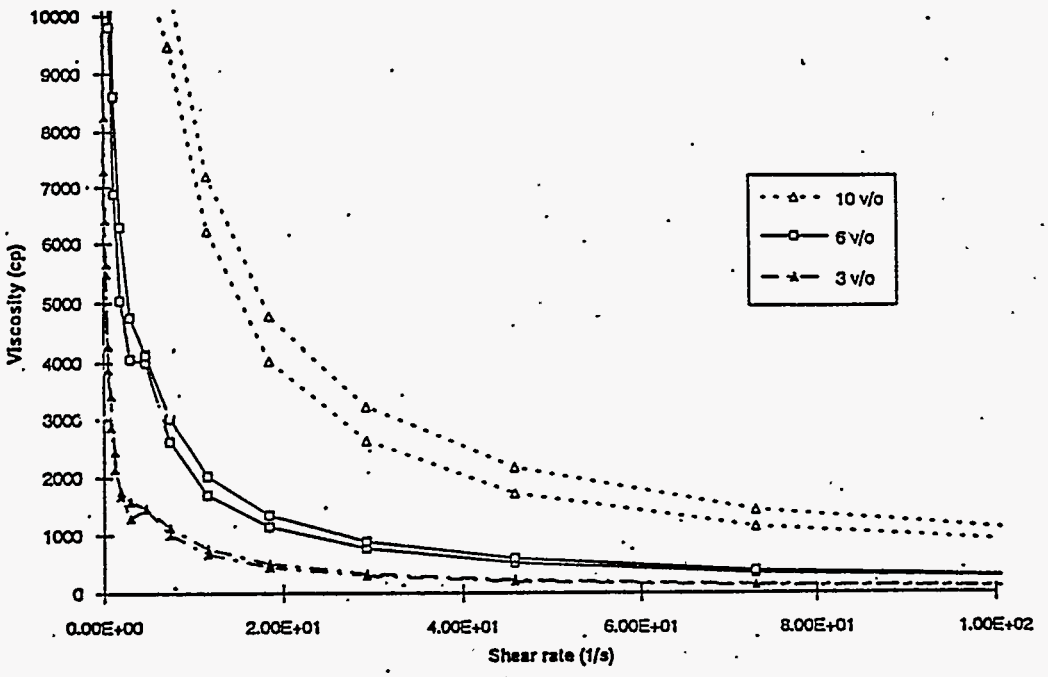

Figure 19. Effective Viscosity of Agglomerated Boehmite Suspensions in a pH10, 0.01 M $NaNO_3$ Solution (stirred for 2 hours)

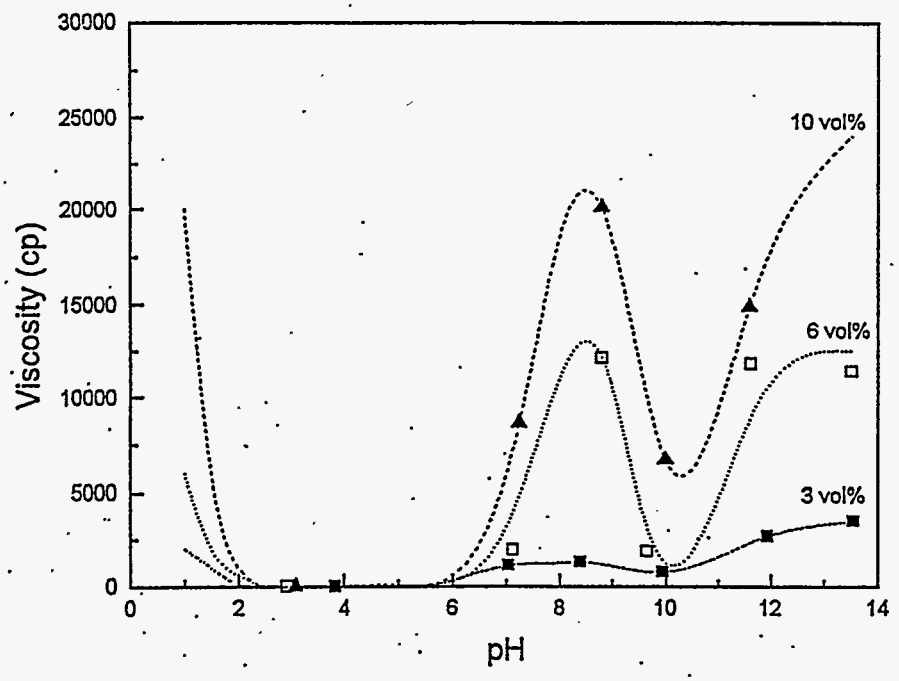

Figure 20. Viscosity of Boehmite Samples with 10^{-2} M $NaNO_3$ as a Function of pH and Solids Loading (shear rate = 11.5 s^{-1})

Viscosities were also measured for boehmite particles suspended in 1 M $NaNO_3$ solutions at different solids loadings. The results are shown in Figure 21. All suspensions in the high salt regime exhibit shear thinning behavior associated with agglomerated particles. Although maxima in the viscosity are still seen at the isoelectric point and at high and low pH, the viscosity is high at all pH values. This is because none of the suspensions in 1 M $NaNO_3$ are dispersed, as predicted in Figure 7. Agglomeration is due to the high ionic strength of the solutions that collapses the electric double layer and inhibits electrostatic stabilization regardless of surface charge. The effect of salt on viscosity is illustrated more directly in Figure 22, which compares the low viscosity, Newtonian behavior of a dispersed boehmite suspension at pH 3 (0.01 M $NaNO_3$ curve) with the highly viscous shear-thinning behavior of a pH 3 slurry agglomerated using 1 M $NaNO_3$.

For sludge processing, the current baseline specifies that slurry viscosities should not exceed 60 cP. Work was conducted to determine the maximum solids loading for boehmite in basic salt-containing solutions (1 M $NaNO_3$, 1 M NaOH) to be encountered in processing. Viscosities of such suspensions as a function of shear rate and solids loading are shown in Figure 23. As expected, the viscosity drops with decreasing solids loading and with increasing shear rate. For shear rates thought to be representative of pumping and transport operations (10-100 s^{-1}), the results show that the solids loading for boehmite suspensions needs to be held below 1 vol% if the maximum desired viscosity is 100 cP. The primary factor that determines the maximum allowable solids loading is the gel point of the colloidal system.

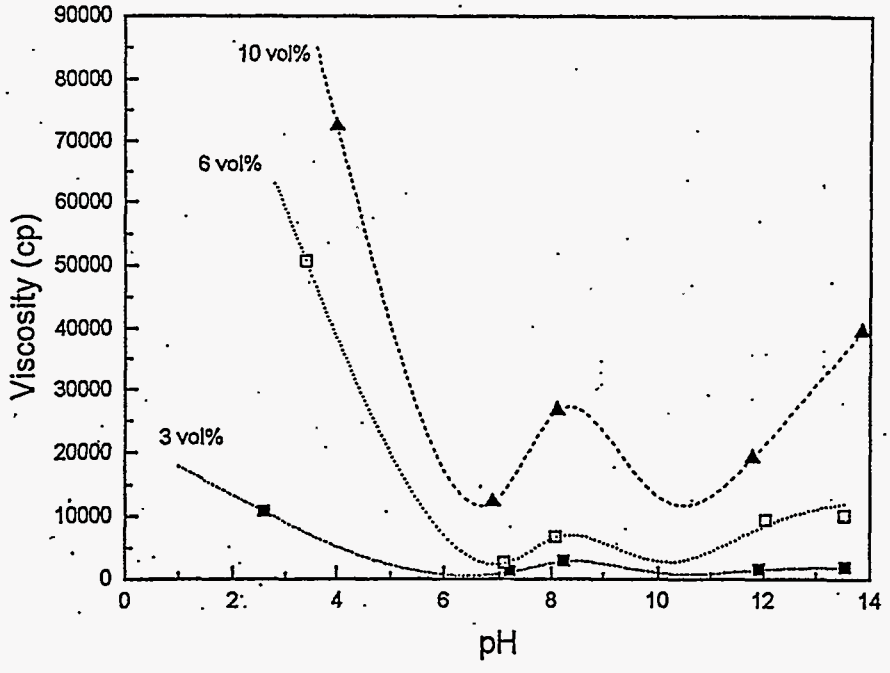

Figure 21. Viscosity of Boehmite Samples with 1 M $NaNO_3$ as a Function of pH and Solids Loading (shear rate = 11.5 s^{-1})

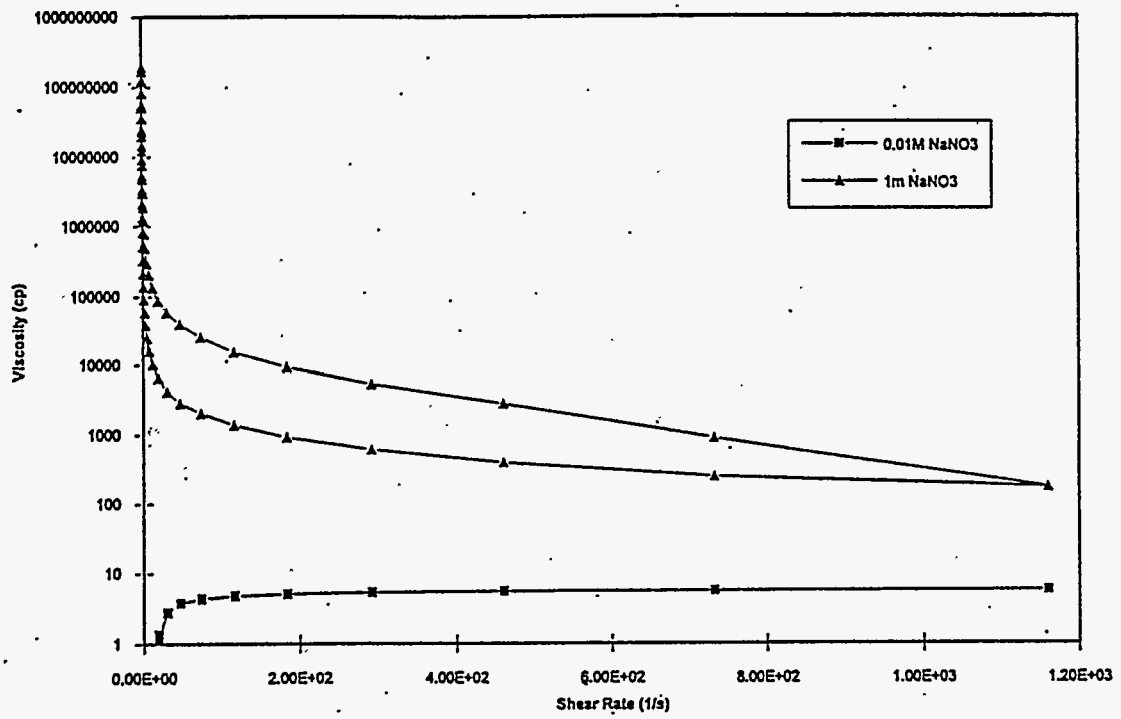

Figure 22. Viscosity vs. Shear Rate for 10 vol% Boehmite Sample at pH = 3

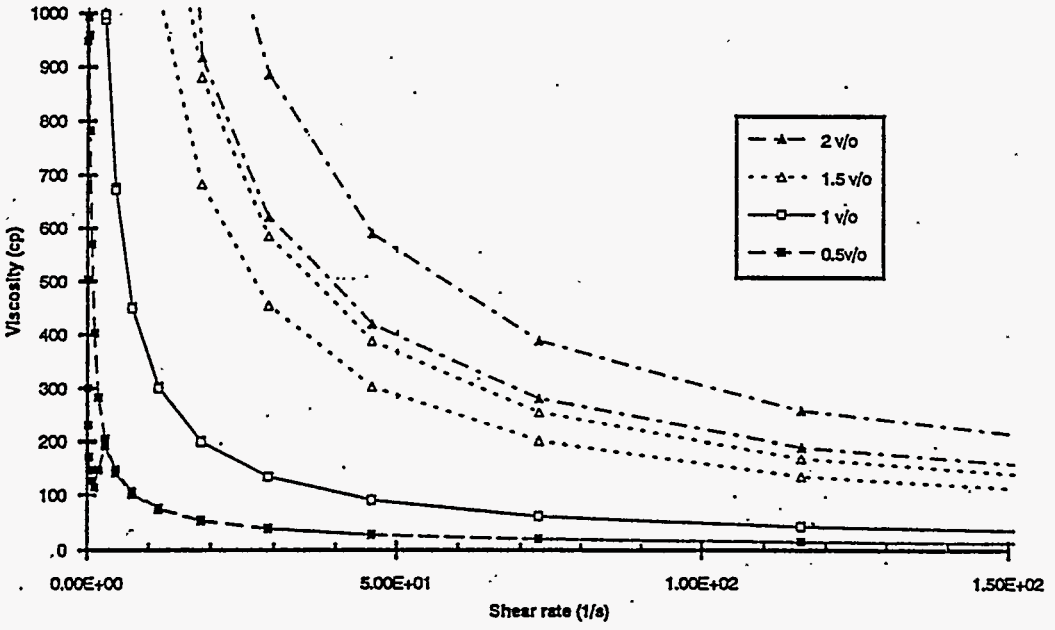

Figure 23. Viscosity of Boehmite at Different Solids Loadings (1 M $NaNO_3$, 1 M NaOH)

4.2 Rheological Models

The ultimate objective of developing computational rheological models is to predict the rheological properties of all colloidal suspensions, including mixtures, under all chemical conditions. To achieve this goal, two separate approaches are being taken:

- Develop a discrete colloidal model that uses information on particle compositions, sizes, interactions, etc. to predict the rheological properties of the suspension from basic principles. (This approach is described in Section 4.2.1.)

- Develop empirical models that can be fitted to experimental data and extrapolated to predict the rheological properties of related suspensions. (This approach is described in Section 4.2.2.)

The rheological properties obtained by either of these methods could then be used in a computational fluid dynamics computer program like TEMPEST (Trent and Eyler 1993) to predict suspension flow in a pipe or a tank.

4.2.1 Discrete Models

In a discreet colloidal model, the motion of each individual colloidal particle is computed. One example of such a model is Stokesian Dynamics (Brady and Bossis 1988) which is similar to classical molecular dynamics in that a system with periodic boundary conditions is filled with a specified number (N) of colloidal particles. The motions of the particles are integrated over a series of time steps and information is obtained from the resulting trajectory. The motions of the particles are influenced by three terms: hydrodynamic interactions, particle-particle force interactions and a Brownian motion term. The hydrodynamic interaction describes how the translational and rotational motion of a particle disturbs the surrounding fluid, which transmits a force to surrounding particles. The most common form of the colloidal particle-particle force interaction is given by DLVO theory, which combines an attractive van der Waals force with a repulsive electrostatic force. When the net potential is attractive, particle collisions result in the formation of colloidal aggregates.

Another example of a discrete model is Brownian Dynamics (TeGrotenhuis, Radke, and Denn 1994), which employs the Langevin equation as the equation of motion for suspended particles. In addition to the hydrodynamic and particle interaction terms, another term is added that represents random fluctuating forces and torques due to collisions with molecules in the suspending medium. However, we have chosen to begin with Stokesian Dynamics in modeling suspension rheology.

Stokesian Dynamics simulations can be used to calculate the viscosity of a colloidal suspension by imposing a fluid shear field on the system and, after the system reaches equilibrium, measuring the bulk stress over a period of time. The particles make three contributions to the bulk stress:

- a mechanical or contact stress transmitted by the fluid due to the shear flow

- an "elastic" stress due to the interparticle forces

- a direct contribution from the Brownian motion.

The simplest system to demonstrate this capability is a two-dimensional system of non-interacting hard spheres suspended in a shearing fluid. The results of these simulations are compared with experimental data in Figure 24. The suspension viscosity is expressed in terms of a relative viscosity, η, which relates it to the viscosity of the base fluid. The solids volume fraction is divided by the maximum packing factor for each system so that the results of the two-dimensional simulation and the three-dimensional experimental data can be compared. Note that the agreement between simulation results and experimental data is excellent. These simulations have been extended to mixed suspensions with particles of different sizes (Chang and Powell 1994).

These results can be extended to colloidal aggregates by assuming that the solid particles are replaced by non-porous, rigid fractal aggregates with the same effective diameter, as a first approximation. The shape of the curve presented in Figure 24 would be the same but the solids volume fraction would be adjusted by the solids density ratio of the solid particles and the fractal aggregates. Because aggregates are porous and flexible, this approach would tend to overestimate the viscosity, assuming no interaction between aggregates. If bonds form between contacting aggregates, a phenomena that occurs at solids concentrations near or above the gel point, the viscosity will be underestimated.

We are extending the discrete model to include DLVO particle-particle interactions. Other terms which must be included before these simulations are performed are bond angle forces to maintain the rigidity of the aggregate structure and bending yield terms. The objective of this activity is to calculate rheological properties of aggregating systems from first principles. The advantage of this approach is that it will be perfectly general in its application and not restricted by a limited base of experimental

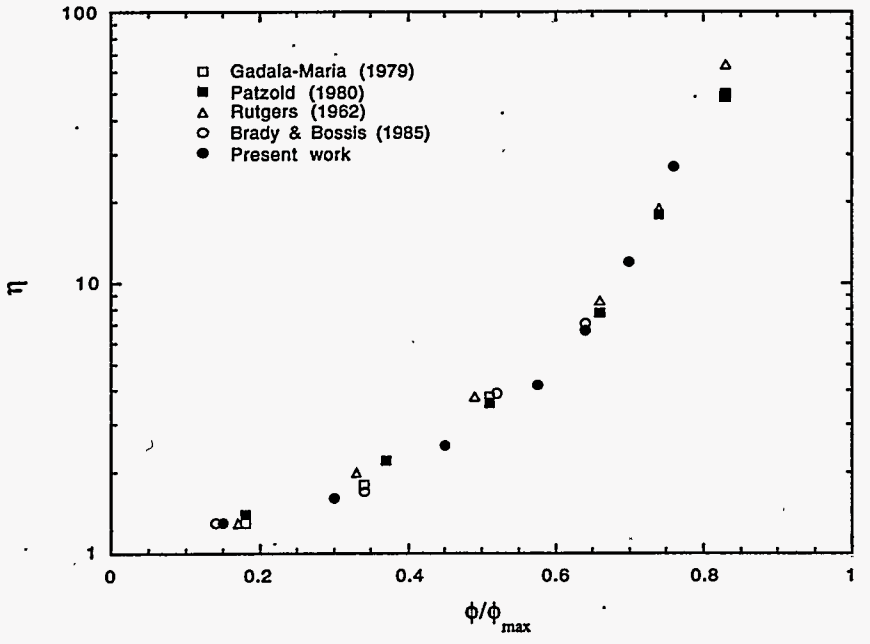

Figure 24. Relative Viscosity as a Function of Volume Fraction

measurements. This is especially important for suspensions of particle mixtures with a large number of particle types, where the number of variables would eliminate any possibility of comprehensively defining every possible system through experiment.

4.2.2 Empirical Models

The other approach to predicting the rheology of colloidal suspensions is to select an empirical relationship to represent a property, like viscosity, in terms of a few adjustable parameters. These parameters can then be related to the properties of the system, such as solids loading, pH, and ionic strength. Once these trends have been established, the information can be used to predict the rheological properties of similar systems.

The rheological behavior of a suspension can be characterized by the shear stress vs. shear strain curve. For simple two-dimensional shear flow in the x-direction, the shear stress (τ_{yx}) is defined as the shear force exerted in the x-direction per unit area. The viscosity of the suspension, η, is defined by the expression

$$\tau_{yx} = -\eta \frac{dv_x}{dy} \tag{21}$$

where v_x is the fluid velocity in the x-direction. Information expressed in terms of shear stress vs. Shear rate can be used in a computational fluid dynamics computer program like TEMPEST to predict suspension flow in a pipe or a tank.

Suspensions of aggregated colloidal particles exhibit different types of behavior. Suspensions with a low solids loadings flow like a fluid for all values of shear stress. Suspensions with a linear relationship between shear stress and shear strain (i.e., η is constant) are called Newtonian fluids. Suspension where the viscosity decreases with increasing shear rate are called pseudoplastic or "shear-thinning" fluids. Some systems with a high solids loading can remain rigid until the shear stress exceeds some yield stress, τ_0, after which it flows like a fluid. Suspensions that exhibit this behavior are called viscoelastic.

Many empirical expressions have been developed to fit the viscometric data of non-Newtonian fluids. Models for pseudoplastic fluids include the power law or Ostwald-DeWaele (Bird et al. 1960), Cross (1965), Carreau (Ellwood et al. 1990), and Biviscous (Kalyon et al. 1993) expressions. Models for viscoelastic materials include the Bingham plastic (Bird et al. 1960), Casson (Bird et al. 1983), Herschel-Bulkley (Bird et al. 1983), and Gay (Dabak and Yucel 1987) expressions. A discussion of these empirical forms is provided in Mahoney and Trent (1995). Two of these expressions, the power law and Bingham plastic, are described in more detail here.

A popular expression describing the shear behavior of pseudoplastic fluids is the power law, or Ostwald-DeWaele, model, which is

$$\tau_{yx} = -m \left| \frac{dv_x}{dy} \right|^{n-1} \frac{dv_x}{dy} \tag{22}$$

where m and n are adjustable parameters. For a Newtonian fluid, n=1 and m=η. For values of n less than unity, the behavior is pseudoplastic. The parameters can be determined by taking the log of Equation 22 to give

$$\ln \tau_{yx} = -\ln m - n \ln \left[\frac{dv_x}{dy}\right] \qquad \text{where } \frac{dv_x}{dy} > 0 \tag{23}$$

and performing a least-squares fit on the data.

The simplest expression that describes the shear behavior of viscoelastic materials is the Bingham plastic model, which is

$$\tau_{yx} = \tau_0 - \mu_0 \frac{dv_x}{dy} \qquad \text{if } |\tau_{yx}| > \tau_0$$
$$\frac{dv_x}{dy} = 0 \qquad \text{if } |\tau_{yx}| < 0 \tag{24}$$

where τ_0 is the yield stress and μ_0 is an adjustable parameter.

The expressions with the least number of adjustable parameters were selected to minimize the uncertainty in fitting the experimental data. As the rheological behavior of specific suspension systems is better understood, empirical expressions with greater detail involving a larger number of parameters may be used.

4.3 Comparison with Experimental Data

The procedure for characterizing the rheological properties of a suspension is to select an empirical model that best fits the data and then fit the parameters for each set of shear stress vs. shear rate data. Once the parameters have been established for a variety of conditions, a functional relationship can be established between these parameters and variables such as solids loadings and solution pH and ionic strength.

The system that we have chosen to illustrate this approach is colloidal boehmite (AlOOH). The effective viscosities as a function of shear rate are shown in Figures 18 and 19 for solutions with pH 3 and pH 10, respectively. As discussed in Section 4.1, the viscosities for the pH 3 solution are nearly constant, indicating Newtonian fluid behavior. The maximum viscosity for each solids loading is shown in Figure 25. Note that the trend in the data is similar to the simulation results for non-interacting particles presented in Figure 24. The primary difference is the scaling with respect to the maximum volume fraction.

The viscosity curves for the pH 10 solution, which are presented in Figure 19, indicate a shear-thinning, pseudoplastic type behavior. This is seen clearly in Figure 26 where the shear stress is plotted as a function of shear rate for 3, 6, and 10 vol% solids loadings. Because the shear stress

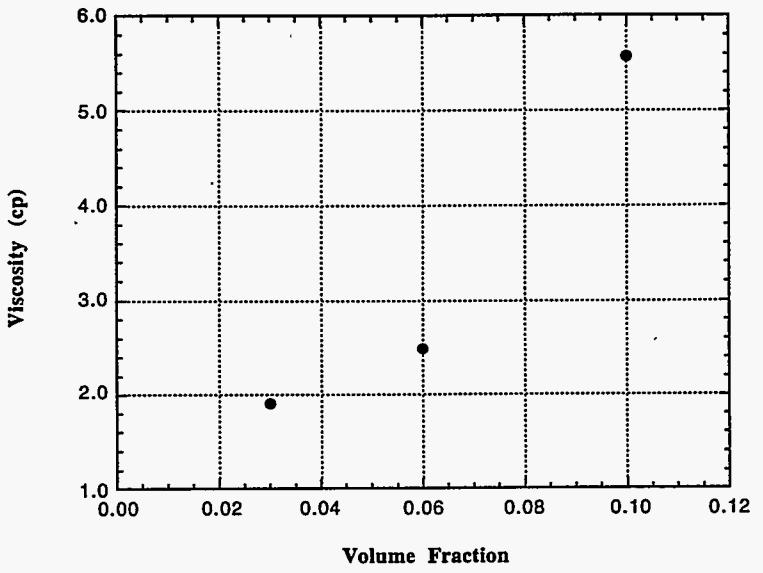

Figure 25. Viscosity of Dispersed Boehmite Suspensions in pH3, 0.01 M $NaNO_3$ Solution

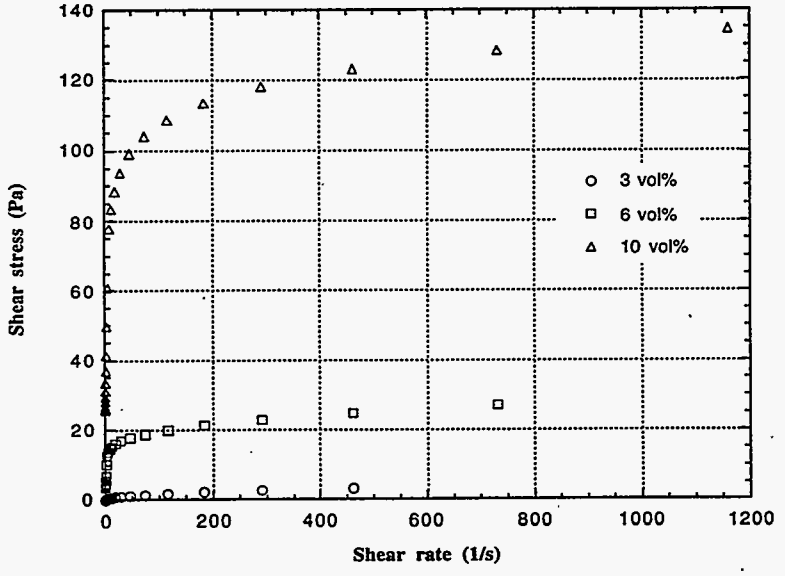

Figure 26. Shear stress vs. Shear Rate for Boehmite Suspensions in pH10, 0.01 M $NaNO_3$ Solution (linear scale)

appears to smoothly approach zero as the shear rate approaches zero, rather than an abrupt yield stress, a pseudoplastic model is probably more appropriate than a viscoelastic model (such as the Bingham plastic).

The suspension exhibits power law behavior if the shear stress vs. shear rate curve plotted on a log-log scale results in a straight line as described by Equation 23. This plot is presented in Figure 27. The shear stress curve can be divided into two regions. Above a transition point between 1 and 10 s^{-1}, the curve appears linear. Below this point, the data appear to level out. This may indicate that for low shear rates, the suspension behaves more like a solid and that the pseudoelastic assumption breaks down. One possible solution may be to use the Herschel-Bulkley model, of which both the power law and Bingham plastic are subsets. For now we will apply the power law expression to the upper half of the curve.

A least-squares fit was performed to determine the appropriate values for m and n for each curve. The resulting curves are compared with the experimental data in Figure 28 for the linear scale and Figure 29 for the log-log scale. The agreement for the linear scale and the upper half of the log-log scale appears to be excellent. Therefore, the parameters used to define these curves may be used as a basis of comparison.

The parameters used in the power law expression are presented in Table 5, along with the equivalent values for pure water. The exponent, n, determines the shape of the curve and, therefore, indicates the degree of pseudoplastic behavior. The value given for water is $n=1$, which is a straight line, indicating a Newtonian fluid. As the solids loading increases, the shape of the curve becomes increasingly non-linear and the value for n monotonically decreases. The lower limit is zero, which would indicate that the shear stress is independent of shear rate.

The parameter m is the scaling factor, which determines the magnitude of the curve. The trend shown in Table 5 is that as the solids loading increases, the magnitude of the curve also increases. This is consistent with the results shown in Figure 25 for dispersed boehmite.

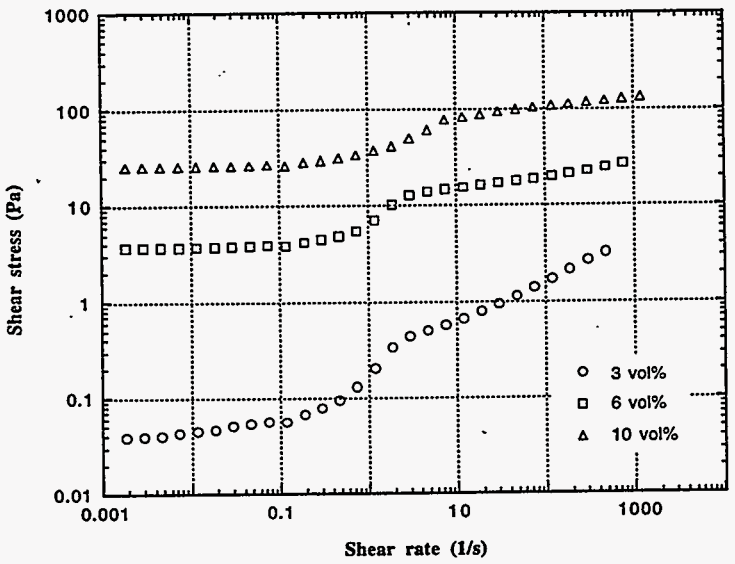

Figure 27. Shear stress vs. Shear Rate for Boehmite Suspensions in pH10, 0.01 M $NaNO_3$ Solution (log scale)

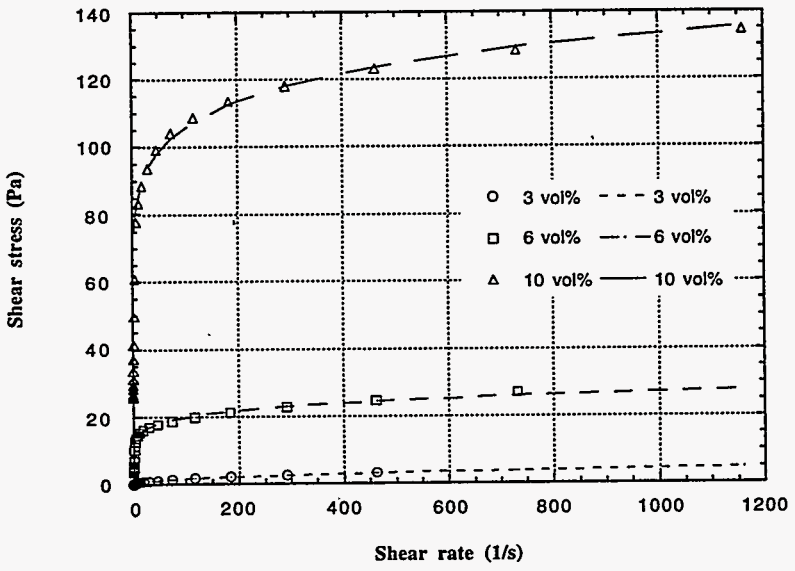

Figure 28. Comparison of Measured and Modeled Shear Stress vs. Shear Rate for Boehmite Suspensions in pH10, 0.01 M $NaNO_3$ Solution (linear scale)

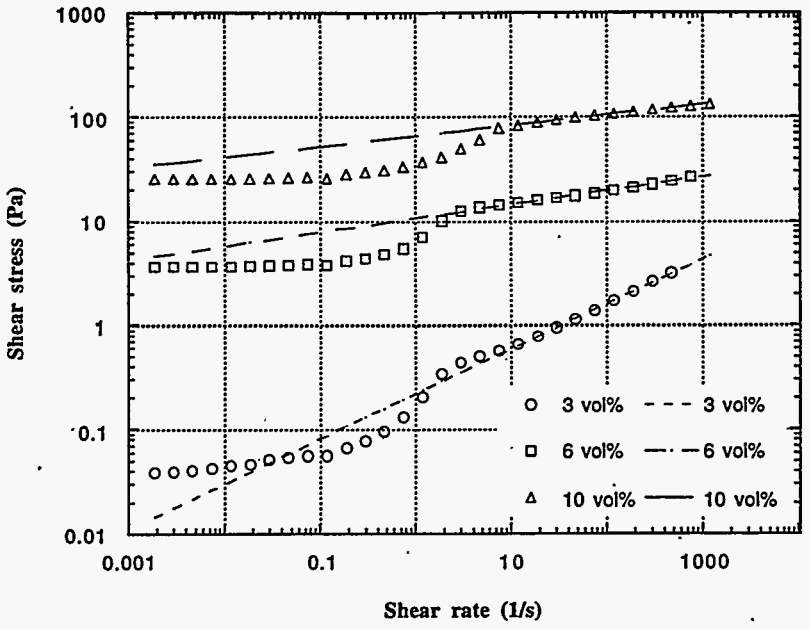

Figure 29. Comparison of Measured and Modeled Shear Stress vs. Shear Rate for Boehmite Suspensions in pH10, 0.01 M $NaNO_3$ Solution (log scale)

Table 5. Parameters for Power Law (Ostwald-DeWaele) Model

Solids Loading	n	m
0 vol%	1.0000	0.0010
3 vol%	0.4323	0.2239
6 vol%	0.1338	10.80
10 vol%	0.1012	66.47

5.0 Conclusions and Recommendations

This report documents the work performed under the Tank Waste Treatment Science task of the TWRS Pretreatment Technology Development Project, which establishes the effect of colloidal agglomeration on the sedimentation and rheological properties of Hanford tank waste, both from an experimental and modeling perspective. Major conclusions resulting from this work are:

- Based on TEM analyses, over half of the insoluble solids in the tank waste examined are in the form of colloidal particles. The major components include the oxides and hydroxides of metals such as aluminum and iron.

- Under certain chemical conditions, these particles aggregate to form fractal clusters that behave much differently from solid particles of the same diameter. The suspension properties depend on the primary particle size, cluster size, and the fractal dimension of the cluster. The cluster size depends on a number of factors, including particle composition, solution pH and ionic strength, and fluid shear.

- Colloidal aggregation affects the sedimentation behavior of a suspension by changing both the settling rate of the suspension and the final sediment density. The settling rate of a cluster can be orders of magnitude greater than that for a primary particle. However, as they settle, the agglomerates may network to form a porous gel with a very low solids density. If the gel point is sufficiently low, the suspension may not settle at all.

- Computational models have been developed that may be used to predict both the equilibrium sediment density profiles and the transient sedimentation behavior of a suspension. The parameters of these models are empirically determined based on benchtop sedimentation experimental data. These models can then be used to predict the behavior of full-scale separation systems.

- The rheological behavior of a suspension depends to a large extent on the degree of colloidal aggregation that has occurred. For non-aggregating particles or very low particle concentrations, the suspension behaves like a Newtonian fluid. When the solids concentration exceeds the gel point, the suspension attempts to form a gel network of interconnecting aggregates and behaves like a shear-thinning liquid. For very low shear rates, particle-particle bonds within the network are broken but then quickly form new bonds. The gel has properties much like an elastic solid. At very high shear rates, the gel network structure is totally disrupted and the suspension behaves like a fluid with a high solids loading.

- Both discrete and empirical computational models have been developed to describe the rheological behavior of aggregating suspensions. The discrete model calculates the rheological properties of a suspension by simulating the detailed motion of individual particles based on hydrodynamic, particle-particle, and Brownian forces. The empirical models are used to predict rheological properties based on experimental data for similar suspensions.

The majority of the work performed under this project was focused on understanding the behavior of simple single-component suspensions. Unfortunately, the Hanford tank wastes contain a complex mixture of submicron particles of different compositions, shapes, and sizes. Experimental studies that we have conducted with suspensions of particle mixtures have shown dramatically different behavior than single-component suspensions of either type of particle. Therefore, the primary recommendation resulting from this work is that both the experimental and modeling efforts be extended to understand and characterize mixed particle systems.

6.0 References

Anderson, D. A., J. C. Tannehill, and R. H. Pletcher. 1984. *Computational Fluid Mechanics and Heat Transfer*. Hemisphere Publishing Corp, New York, New York.

Bird, R. B., G. C. Dai, and B. J. Yarusso. 1983. "The Rheology and Flow of Viscoplastic Materials," *Rev. Chem. Eng.*, **1**, 1.

Bird, R. B., W. E. Stewart, and E. N. Lightfoot. 1960. *Transport Phenomena*. John Wiley & Sons, Inc., New York, New York.

Brady, J. F. and G. Bossis. 1985. "The Rheology of Concentrated Suspensions of Spheres in Simple Shear Flow by Numerical Simulation," *J. Fluid Mech.*, **155**, 105.

Brady, J. F. and G. Bossis. 1988. "Stokesian Dynamics," *Ann. Rev. Fluid. Mech.*, 20, 111.

Buscall, R., I. J. McGowan, P.D.A. Mills, R. F. Stewart, D. Sutton, L. R. White, and G. E. Yates. 1987. "The Rheology of Strongly Flocculated Suspensions," *J. Non-Newtonian Fluid Mech.*, **24**, 183.

Buscall, R. and L. R. White. 1987. "The Consolidation of Concentrated Suspensions: Part 1 - The Theory of Sedimentation," *J. Chem. Soc., Faraday Trans. I*, **83**, 873.

Chang, C. and R. L. Powell. 1994. "Effect of Particle Size Distributions on the Rheology of Concentrated Bimodal Suspensions," *J. Rheol.*, **38**, 85.

Cross, M. M. 1965. "Rheology of Non-Newtonian Fluids: A New Flow Equation for Pseudoplastic Systems," *J. Colloid Sci.*, **20**, 417.

Dabak, T. and O. Yucel. 1987. "Modeling of the Concentration and Particle Size Distribution Effects on the Rheology of Highly Concentrated Suspensions," *Powder Tech.*, **52**, 193.

DeGuingand, N. J. 1986. "The Behavior of Flocculated Suspensions in Compression," M.E. Thesis, Univ. Melbourne, Australia.

Ellwood, K.R.J., G. C. Georgiou, T. C. Papanastasiou, and J. O. Wilkes. 1990. "Laminar Jets of Bingham-plastic Liquids," *J. Rheol.*, **34**, 787.

Gadala-Maria, F. A. 1979. "The Rheology of Concentrated Suspensions," Ph.D. Thesis, Stanford University, Stanford, California.

Honig, E. P., G. J. Roebersen, and P. H. Wiersema. 1971. *J. Colloid Interface Sci.*, **36**, 97.

Hunter, R. J. 1986. *Foundations of Colloid Science*. Clarendon Press.

Kalyon, D. M., P. Yaras, B. Aral and U. Yilmazer. 1993. "Rheological Behavior of a Concentrated Suspension: A Solid Rocket Fuel Simulant," *J. Rheol.*, **37**, 35.

LaFemina, J. P. et al. 1995a. *Tank Waste Treatment Science: Report for the First Quarter FY 1995.* PNL-10762, Pacific Northwest Laboraory, Richland, Washington.

LaFemina, J. P. et al. 1995b. *Tank Waste Treatment Science: Report for the Second Quarter FY 1995.* PNL-10763, Pacific Northwest Laboraory, Richland, Washington.

LaFemina, J. P. et al. 1995c. *Tank Waste Treatment Science: Report for the Third Quarter FY 1995.* PNL-10764, Pacific Northwest Laboraory, Richland, Washington.

Landman, K. A., L. R. White, and R. Buscall. 1988. "The Continuous-Flow Gravity Thickener: Steady State Behavior," *AIChE J.*, **34**, 239.

Mahoney, L. A. and D. S. Trent. 1995. *Correlation Models for Waste Tank Sludges and Slurries.* PNL-10695, Pacific Northwest Laboratory, Richland, Washington.

Orme, R. M. "Chemical and Radionuclide Inventory for Single and Double-Shell Tanks," WHC-SD-WM-TI-613, Rev. 1, dated August 7, 1995, Westinghouse Hanford Company, Richland, Washington.

Rapko, B. M., G. J. Lumetta, and M. J. Wagner. 1995. *Washing and Caustic Leaching of Hanford Tank Sludges: Results of FY 1995 Studies*. PNL-10712, Pacific Northwest Laboratory, Richland, Washington.

Russel, W. B., D. A. Saville, and W. R. Schowalter. 1989. *Colloidal Dispersions*. Cambridge University Press, Cambridge.

Rutgers, R. 1962. "Relative Viscosity of Suspensions of Rigid Spheres in Newtonian Liquids," *Rheol. Acta*, **2**, 202.

Sonntag, H. and K. Strenge. 1986. *Coagulation Kinetics and Structure Formation*. Plenum Press.

TeGrotenhuis, W. E., C. J. Radke, and M. M. Denn. 1994. "Brownian Dynamics of Sterically-Stabilized Colloidal Suspensions," *AIChE J.*, **40**, 283.

Trent, D. S. and L. L. Eyler. 1993. *TEMPEST: A Computer Program for Three-Dimensional Time-Dependent Computational Fluid Dynamics. Volume 1: Theory. Version T, Mod 2.* PNL-8857, Rev. 0, Pacific Northwest Laboratories, Richland, Washington.

Von Smoluchowski, M. 1917. *Z. Phys. Chem.*, **92**, 129.